Cirrus parcel model comparison project phase 1: The critical components to simulate cirrus initiation explicitly

Ruei-Fong Lin[1], David O'C. Starr[2], Paul J. DeMott[3], Richard Cotton[4], Kenneth Sassen[5], and Eric Jensen[6]

[1]UMBC/GEST Center, Baltimore, MD, USA

[2]Laboratory of Atmosphere, NASA/GSFC, Greenbelt, MD, USA

[3]Dept. of Atmospheric Sciences, Colorado State University, Fort Collins , CO, USA

[4]Meteorological Research Flight, Hants, UK

[5]Dept. of Meteorology, University of Utah, UT, USA

[6]NASA/Ames Research Center, Moffett Field, CA, USA

Submitted to *J. Atmos. Sci.*

Corresponding author address: Ruei-Fong Lin

UMBC/GEST Center

NASA/GSFC, Code 912

Greenbelt, MD, 20771

E-mail: lin@agnes.gsfc.nasa.gov

Abstract

The Cirrus Parcel Model Comparison Project, a project of the GCSS (GEWEX Cloud System Studies) Working Group on Cirrus Cloud Systems, involves the systematic comparison of current models of ice crystal nucleation and growth for specified, typical, cirrus cloud environments. In Phase 1 of the project reported here, simulated cirrus cloud microphysical properties are compared for situations of "warm" (-40°C) and "cold" (-60°C) cirrus, both subject to updrafts of 4, 20 and 100 cm s^{-1}. Five models participated. The various models employ explicit microphysical schemes wherein the size distribution of each class of particles (aerosols and ice crystals) is resolved into bins or treated separately. Simulations are made including both the homogeneous and heterogeneous ice nucleation mechanisms. A single initial aerosol population of sulfuric acid particles is prescribed for all simulations. To isolate the treatment of the homogeneous freezing (of haze droplets) nucleation process, the heterogeneous nucleation mechanism is disabled for a second parallel set of simulations.

Qualitative agreement is found for the homogeneous-nucleation-only simulations, e.g., the number density of nucleated ice crystals increases with the strength of the prescribed updraft. However, significant quantitative differences are found. Detailed analysis reveals that the homogeneous nucleation rate, haze particle solution concentration, and water vapor uptake rate by ice crystal growth (particularly as controlled by the deposition coefficient) are critical components that lead to differences in predicted microphysics.

Systematic bias exists between results based on a modified classical theory approach and models using an effective freezing temperature approach to the treatment of nucleation. Each approach is constrained by critical freezing data from laboratory studies,

but each includes assumptions that can only be justified by further laboratory research. Consequently, it is not yet clear if the two approaches can be made consistent. Large haze particles may deviate considerably from equilibrium size in moderate to strong updrafts (20-100 cm s^{-1}) at -60°C when the commonly invoked equilibrium assumption is lifted. The resulting difference in particle-size-dependent solution concentration of haze particles may significantly affect the ice particle formation rate during the initial nucleation interval. The uptake rate for water vapor excess by ice crystals is another key component regulating the total number of nucleated ice crystals. This rate, the product of particle number concentration and ice crystal diffusional growth rate, which is particularly sensitive to the deposition coefficient when ice particles are small, modulates the peak particle formation rate achieved in an air parcel and the duration of the active nucleation time period.

The effects of heterogeneous nucleation are most pronounced in weak updraft situations. Vapor competition by the heterogeneously nucleated ice crystals may limit the achieved ice supersaturation and thus suppresses the contribution of homogeneous nucleation. Correspondingly, ice crystal number density is markedly reduced. Definitive laboratory and atmospheric benchmark data are needed for the heterogeneous nucleation process. Inter-model differences are correspondingly greater than in the case of the homogeneous nucleation process acting alone.

1. Introduction

The Cirrus Parcel Model Comparison Project (CPMC) is a project of the GEWEX (Global Energy and Water Cycle Experiment) Cloud System Study Program (GCSS) Working Group on Cirrus Cloud Systems (WG2). The primary goals of this project are to assess the current understanding of cirrus microphysical modeling and to identify cirrus model sensitivities to the state of our knowledge of nucleation and microphysics at low temperature. CPMC also gives the Idealized Cirrus Model Comparison Project (ICMCP) of GCSS WG2 a benchmark estimate of the cirrus initiation characteristics. Furthermore, the findings of this project are expected to provide improvements for models with simpler cirrus microphysical modules.

Simulations of cloud initiation processes and the evolution of hydrometeor size distribution by explicit microphysical schemes date back to the 1940s and 50s (e.g., Howell 1948; Mordy 1958). The direct application of explicit microphysical schemes to simulate cirrus clouds did not begin until the late 1980s after the vast area-coverage of cirrus was recognized, and the effects of cirrus on the global radiation budget were addressed (e.g., Liou 1986; Ramanathan et al. 1989). Sassen and Dodd (1988) compared lidar data with parcel model results to infer the homogeneous nucleation rate of ice in supercooled cloud droplets within the temperature range of -34.3° and -37.3°C. Heymsfield and Sabin (1989) conducted a numerical study of homogeneous freezing of ammonium sulfate solution droplets at water subsaturated conditions between -40° and -50°C. They reported that the predicted number concentration of ice crystal depended on temperature, parcel cooling rate, and cloud condensation nuclei (CCN) distributions. Parameterization of homogeneous freezing of supercooled cloud droplets and CCN solution droplets for

use in regional-scale cloud models via a bulk microphysical scheme was developed with the aid of parcel model simulations (DeMott et al. 1994). These simulations relied on an explicit microphysical scheme, in which the number distribution of ice particles is resolved into bins, in contrast to the use of bulk parameterizations. The parcel model approach was also adopted in evaluating the potential impact of volcanic aerosols on cirrus microphysics (Jensen and Toon 1992), and in the study of orographic clouds where laminar flow produces these clouds. For example, model results were compared with *in situ* measurements of orographic clouds (Jensen et al. 1998; Lin et al. 1998), and the dominant nucleation mode under various background conditions was investigated (Spice et al. 1999; DeMott et al. 1997).

Jensen et al. (1994a,b) used a one-dimensional model, which included the vertical transport of particles, to study the initiation as well as the development of cirrus. Model results were sensitive to parameters controlling the homogeneous nucleation rate; namely, the activation energy and ice-solution surface tension. These and other authors (Heymsfield and Sabin 1989; DeMott et al. 1994) have also demonstrated that cirrus microphysical properties, unlike those of stratus, are not very sensitive to the total CCN number concentration. This is a consequence of (i) the fact that homogeneous nucleation of ice in supercooled solution droplets acts first and foremost on the larger end of the CCN size distribution, and (ii) the fraction of the CCN population that participates in homogeneous freezing is usually quite small, being vapor-limited by the ice formation process itself. Explicit microphysical schemes have been incorporated into fully-coupled multi-dimensional models to investigate contrail evolution (Gierens and Jensen 1996; Khvorostyanov and Sassen 1998c), dynamic-radiative-microphysical interaction in cirrus

anvils (Lin 1997), and fundamental issues of nucleation and ice particle growth with implications for cirrus cloud development (Khvorostyanov and Sassen 1998a).

Many studies have ignored heterogeneous nucleation as a mechanism for cirrus formation, primarily because of the current lack of knowledge regarding the abundance and activation of ice nuclei in the upper troposphere. However, it is becoming apparent that the conditions observed for cirrus formation (Heymsfield and Miloshevich 1995; Heymsfield et al. 1998) cannot be satisfied by simply incorporating the existing knowledge of the freezing of sulfate particles via homogeneous freezing schemes (DeMott 2001). This differs from conclusions that were initially inferred from model findings by Heymsfield and Miloshevich (1993). Sassen and Benson (2000) indicated that heterogeneous ice nucleation can strongly modulate the cirrus formation process, but only if ice nuclei concentrations and activations are similar to the most favorable conditions measured at the Earth's surface. So, heterogeneous nucleation must ultimately be parameterized in some manner. This project attempts to clarify the range of effects to be expected from incorporating various available heterogeneous nucleation schemes that are either based on data or expectations.

Qualitative agreement between models are frequently demonstrated in the papers cited above; however, the quantitative discrepancy margin has yet to be assessed. It is important to do a systematic comparison of these models because of the sensitivity of cloud microphysical and radiative properties to the cloud initiation processes. The questions we hope to answer from this exercise are; what is the range of model responses to a highly-idealized situation; what are the key components in the models causing discrepancies in the simulation results; and what kind of bias would these discrepancies

introduce if various microphysical schemes are adopted in multi-dimensional models.

The intercomparison study described here took place at the GCSS WG2 workshop at Geestatch, Germany on 19-21 May 1999. Five parcel modeling groups from the UK and USA participated in the intercomparison. A brief description of the participant models is given in Section 3.

Participants were asked to submit a series of relatively simple calculations involving an ascending parcel lifted by a superimposed updraft without mass and heat exchange with the environment. The primary focus was on the homogeneous nucleation process operating in isolation (hereafter, HN-ONLY). A secondary focus was the combination of the homogeneous and heterogeneous ice nucleation mechanisms included in cirrus parcel models (hereafter, ALL-MODE). A detailed description of the project is given in Section 2. Cirrus initiation requirements and cloud properties are presented and the implications of the model results discussed in Section 4 followed by a summary in Section 5.

2. Simulation protocols

We focus on the nucleation regimes of the warm and cold cases studied in the WG2 ICMCP (Starr et al. 2000), and test the models under a range of imposed updraft conditions (0.04, 0.2, 1 m s^{-1}). All parcel models were run in the "closed" Lagrangian mode, i.e., neither particle fallout nor mixing with the environment was allowed. Nucleation and ice crystal growth were forced through an externally imposed constant rate of lift, W, with consequent adiabatic cooling. The parcel cooling rate is formulated as

$$\frac{dT}{dt} = -\frac{g}{C_p}W + \dot{Q}_{LH}. \tag{1}$$

where $\dot{Q}_{LH}$ is the latent heat release due to diffusional growth of hydrometeors. The environmental pressure was specified as:

$$\frac{d \ln P}{dz} = -\frac{g}{R_d[T_{ini} - \Gamma(z - z_{ini})]}, \tag{2}$$

where the environmental lapse rate, Γ, approximates the ice pseudo-adiabatic lapse rate for the assumed conditions. The background haze particles[1] are assumed to be aqueous sulfuric acid particles with a number concentration of 200 cm^{-3}, lognormally distributed with a pure H_2SO_4 mode radius of 0.02 micron and a distribution width corresponding to $\sigma = 2.3$ with pure H_2SO_4 density as 1.841 g cm^{-3}. The initial conditions for the 14 runs are tabulated in Table 1. In each of the HN-ONLY runs (Wh004, Wh020, Wh100, Ch004, Ch020, and Ch100), only homogeneous nucleation mode is allowed to form ice crystals; the other mode is turned off. Both nucleation modes are switched on in ALL-MODE runs (Wa004, Wa020, Wa100, Ca004, Ca020, and Ca100). Participants were asked to run two additional simulations, Wh020L and Ch020L, by setting $\lambda = 2$ (to be discussed further in Section 3a), or tailoring the nucleation rate calculation so that the predicted freezing is in agreement with $\lambda = 2$. Chen et al. (2000) noted that $\lambda = 2$ agreed with their data, and those presented by Koop et al. (1998). This same λ, or equivalent theoretical treatment, served as a tool to diagnose the relative importance of nucleation rate versus the treatment of haze and ice particle growth in determining the source of model differences in the predicted N_i.

Heterogeneous nucleation could be the dominant ice formation mode in cirrus in slow updraft conditions (e.g., DeMott et al. 1997; Spice et al. 1999; Sassen and Benson 2000).

---

[1]Similar aerosol number distribution was used in Jensen et al. (1994a).

However, significant differences exist in treatments of the heterogeneous ice nucleation processes. Thus, major inter-model differences might be expected in the predicted cirrus microphysical properties. Definitive laboratory and atmospheric benchmark data are only now being developed. Despite the still primitive nature of this subject, it is important to compare the frequently used schemes and assess their features.

The shape of ice crystals may also affect the simulation. In order to simplify the comparison, participants assumed ice crystals to be spherical with constant ice density of 0.9 g cm^{-3}. The assumption of bulk ice density may be an acceptable approximation for the small crystal sizes present in most of the simulations (e.g., Heymsfield and Sabin 1989), but it is expected that the simulation results will be sensitive to this assumption (Heymsfield, personal communication). Participants also assured that time steps were small enough not to cause numerical artifacts. For the present calculations, ice particle aggregation and direct radiation effect on diffusional growth are ignored.

The depth of parcel lift used in this study was set to assure that parcels underwent complete transition through the nucleation regime to a stage of approximate equilibrium between ice mass growth and vapor supplied by the specified updrafts. This was deemed to provide the best comparison of the models and their sensitivities to critical parameters.

3. Model descriptions

A brief summary of the model characteristics is given in Table 2. Hereafter, we will refer to these models as the C, D, J, L, S models, respectively, as denoted in the table. According to the method in which particles are handled, these models are classified as either particle-tracing models or bin models (Young 1993). In the particle-tracing method,

the evolution of each individual particle is traced (model S). In bin models (models C, D, J and L), particles are grouped according to particle size or mass to expedite numerical integration. Individual particle histories are lost in the grouping process. Among the five models, J and L have been incorporated into fully-coupled multi-dimensional models. The major components in parcel models, from a numerical standpoint, are the time-integration scheme and size-coordinate scheme. From the standpoint of cloud physics, the major components are the specification and treatment of the saturation vapor pressure, diffusional growth of ice and haze particles, equilibrium haze size and solution concentration, and heterogeneous and homogeneous nucleation schemes (Fig. 1). The latter three components are highlighted in this section.

a. Homogeneous nucleation of unactivated solution particles

Much progress has been made in estimating homogeneous nucleation rate of ice in pure water droplets, J_w, by theoretical, laboratory and field measurement studies (e.g., Sassen and Dodd 1988; DeMott and Rogers 1990; Pruppacher 1995; Jeffery and Austin 1997). The nucleation rate J_w can be formulated theoretically or fitted parametrically to droplet temperature only (e.g., Heymsfield and Sabin 1989; Jeffery and Austin 1997; and Khvorostyanov and Sassen 1998b). Consensus on the temperature dependence of J_w in the temperature regime where pure water freezes homogeneously has been reached in the community. The estimate of the nucleation rate of ice in solution droplets, J_{haze}, however, remains an active research area. This is critically important for cirrus modeling because most cirrus clouds form below the homogeneous freezing temperature of pure water ($\sim -40°C$) and at relative humidities below saturation with respect to the liquid

phase, where liquid water exists only as a component of solution droplets.

The homogeneous nucleation rate of ice in solution droplets has been derived in various studies using (i) the modified classical theory approach (model J) or (ii) an empirical approach referred to as the effective freezing temperature (hereafter, T_{eff} approach, models C, D, L, and S). In either case, calculations depend critically on the use of laboratory data describing properties of solution particles at cirrus temperatures. The modified classical theory approach computes nucleation rate using the equation (Pruppacher and Klett 1997)

$$J_{haze} = 2N_c(\frac{\rho_w B_z T}{\rho_i h})(\frac{\sigma_{i/s}}{B_z T})^{1/2} \exp[-\frac{(\Delta F_{actv} + \Delta F_{germ})}{B_z T}], \quad (3)$$

where $\sigma_{i/s}$, ΔF_{actv}, and $\Delta F_{germ} = \frac{4\pi\sigma_{i/s}}{3}(\frac{2\sigma_{i/s}}{\overline{\rho_i}(\overline{L_m}\ln(T_0/T)+\frac{1}{2}(T_0+T)R_v \ln a_w)})^2$ are the surface tension across the ice-solution interface, activation energy, and ice-germ formation energy, respectively. All symbols are defined in Notation. Solution effects, primarily compositional effects on $\sigma_{i/s}$, serve to raise the critical germ radius and the required germ formation energy. In order to use (3), laboratory data on $\sigma_{i/s}$ and ΔF_{actv} as functions of temperature and composition are needed. Seldom are both quantities available from direct measurement for a given solution. Typically, direct data on one parameter is used and the other is constrained by measurements of J_{haze}. Thus, in model J, recent direct data on $\sigma_{i/s}$ was incorporated and ΔF_{actv} was inferred from laboratory measurements of J_{haze} for sulfuric acid haze particles following the method of Tabazadeh et al. (2000).

The T_{eff} approach attempts to directly link measured nucleation rates of ice in solution particles to nucleation rates of equivalent-sized pure water droplets via a

parameter called the effective freezing temperature. T_{eff} is defined as

$$T_{eff} = T + \lambda \Delta T_m, \tag{4}$$

as introduced by Sassen and Dodd (1988) such that

$$J_{haze} = J_w(T_{eff}). \tag{5}$$

In (4), ΔT_m is the equilibrium melting point depression (positive valued), which depends on solution concentration, and λ is an empirical coefficient to account for additional suppression ($\lambda > 1$) or enhancement ($\lambda < 1$) of nucleation (freezing) temperature due to non-ideal interaction between ions and condensed water. Nucleation rate is extremely sensitive to ΔT_m and λ; thus, these two factors must be specified with care. The values of λ are constrained by, and in fact have their source in, laboratory data, as first described by Sassen and Dodd (1988). Although Sassen and Dodd (1988) noted that an average λ for different solutions was around 1.7, the value for specific solutions may range from just greater than 1 to about 2.5 (DeMott 2001). The existence of relation (4) as a descriptor of laboratory data on the freezing of a large variety of solution droplet types has never been explained theoretically from first principles.

The homogeneous nucleation rates for sulfuric acid solution droplets computed by these methods are compared as functions of temperature in Figure 2. In this figure, the same equilibrium-sized haze particle data provided by Paul DeMott is used in each model where λ is set to 2 and the fitted ΔT_m by DeMott et al. (1997) is adopted. The curves for models using the T_{eff} approach agree fairly well, e.g., 1°C difference in temperature where $J_{haze}V = 1$ s^{-1} for a 5% weight percent solution droplet. This is not surprising because, as long as these schemes use an identical value of λ and the same formula to compute

ΔT_m, the differences in nucleation rate is solely determined by the differences in the functional specification of the homogeneous nucleation rate of ice in pure water J_w. This figure suggests that, at the critical freezing condition ($J_{haze}V = 1$ s^{-1}), the formulation differences for J_w in the T_{eff} group at most contribute an absolute 1% difference in the critical solute weight percent (hereafter wt%) .

The classical approach to determine J_{haze}, as in model J, can be interpreted as a T_{eff} scheme with varying λ. Given temperature, the classical approach would obtain smaller $J_{haze}V$ compared to the T_{eff} approach when solution is dilute (e.g., T = -45°C, wt% = 5). The opposite is found when solution is more concentrated (e.g., T = -45°C, wt% = 15). Given solute wt%, model J produces larger $J_{haze}V$ than those using T_{eff} approach when temperature is warm (e.g., T = -35°C, wt% = 5). The condition reverses as temperature decreases (e.g., T = -45°C, wt% = 5). Therefore, the intrinsic λ in the classical approach varies inversely with solution concentration and temperature (Fig. 3). Also following this figure, the inferred $\lambda\Delta T_m$ from model J at these two temperature regions does not approach 0 as solute wt% decreases to 0. This may be a potential problem.

For a given temperature, $J_{haze}V$ computed by the two approaches shows high sensitivity to the haze particle solute wt% (Fig. 2). However, the gradient of $J_{haze}V$ to solute wt% in the T_{eff} approach is much greater. For instance, at T=-45°C, $J_{haze}V$ computed by model J ranges roughly from 10^{-8} to 1 s^{-1} for solute wt% from 15 to 5%; whereas the T_{eff} approach models render a range from 10^{-21} to 10 s^{-1} for the same solute wt% range. In the next section, we will show that this difference in the sensitivity of $J_{haze}V$ to solution concentration is the dominant factor leading to the systematic differences in the freezing haze size distributions between the two approaches.

It is not known if the behavior predicted by classical nucleation theory as treated in model J is a consequence of the way that theory was constrained by a single laboratory data set, or if it reflects a real expected consequence of solution effects on freezing. Laboratory measurements usually focus on the $J_{haze}V = 1$ s^{-1} region. Nucleation rate data over a wide range of values, particularly data points beyond the critical freezing condition, are needed for solutions of similar composition to address this issue.

Differences in λ affect the required humidity to trigger nucleation. If λ is the only varying component, it's expected that homogeneous nucleation is first triggered in the model with the smallest λ because particles freeze at higher solute wt% which entails a lower RH_w condition. Therefore, the range of wt% correspond to a given $\lambda\Delta T_m$ might be used to estimate the triggering RH_w condition, at least, to a first order basis. It is shown from Fig. 3 that this wt% range increases with $\lambda\Delta T_m$. Meanwhile, the required $\lambda\Delta T_m$ to trigger nucleation increases with a decrease in temperature. We may then conclude that the nucleation triggering RH_w becomes more sensitive to λ as temperature decreases. This will be further demonstrated in the model results (Section 4).

b. Heterogeneous nucleation

Little constraint was imposed on formulating heterogeneous nucleation because theoretical and experimental understanding is still quite poor. For the ALL-MODE simulations, both parameterized and explicit heterogeneous nucleation calculation are used. Models C and L employ ice saturation ratio dependent parameterizations of activated IN as

$$N_{IN} = A(S_i - 1)^B, \tag{6}$$

following Spice et al. (1999); and

$$N_{IN} = \exp[\alpha + 100\beta(S_i - 1)], \tag{7}$$

following Meyers et al. (1992), respectively. Note that the values of the coefficients mentioned in this section are listed in Notation. Hence, number concentrations of ice crystals produced by heterogeneous nucleation are controlled solely by the peak S_i in the simulations.

At relatively high peak S_i condition, the parameterized N_{IN} by these two formulas may exceed the range of 0.1 to 100 L^{-1} measured by Rogers et al. (1998) from aircraft, c.f., N_{IN} becomes 1000 L^{-1} when S_i is 1.38 (Eq. 6) or 1.48 (Eq. 7). Although most of the flights were spent at temperature between -35 to -60°C, Rogers et al. (1998) processed conditions from about -15 to -40°C and from ice saturation to ~15% water supersaturation. Since activation of IN depends on temperature and humidity, it is possible that more IN are active at lower temperature than those considered in the measurements by Rogers et al. (1998). Nevertheless, the formulas Eq. 6 and 7 are expected to represent a maximum heterogeneous nucleation impact.

Models D and S treat heterogeneous freezing in an explicit fashion. Haze particles of the given H_2SO_4 aerosol distribution are subject simultaneously to heterogeneous and homogeneous nucleation. The unfrozen haze particles are tracked during the entire simulation. Model D assumes that all heterogeneous ice nuclei were freezing nuclei contained within 10% of the cloud condensation nuclei (CCN) population at sizes above 0.1 μm. Further, these particles were assumed to contain 50% insoluble matter (bulk density of 1.9 g cm^{-3}), the rest being H_2SO_4. These choices have a basis in observations

from DeMott et al. (1998) at temperatures down to -35°C. The average freezing nuclei spectrum from that study was employed and extrapolated to cirrus temperatures in this study. Thus, the fraction of ice nuclei from each haze category k ($> 0.1\mu$m) were predicted according to

$$F_k = \frac{a}{F_{>0.1\mu m}}(T_0 - T_{eff,k})^b, \tag{8}$$

where $F_{>0.1\mu m}$ is the fraction of CCN with size greater than 0.1 μm compared to the total CCN. This treatment was expected to yield the most conservative (minimal) estimate of heterogeneous ice nuclei concentrations in cirrus.

Model S assumes that the ice particle formation due to heterogeneous nucleation follows a T_{eff} modified Fletcher function given by Khvorostyanov and Sassen (1998a) as

$$\frac{dN_i}{dt} = \sum_k A_{s0} B_s \exp(-A_z z) \exp[B_s(T_0 - T_{eff,k})] \frac{dT}{dt}. \tag{9}$$

Note that this equation introduces a height dependent term into the concentration of ice nuclei in the upper troposphere. A higher than normal value of B_s (0.8 compared to 0.4 to 0.6 of the "typical cirrus" in Sassen and Benson (2000)) is arbitrarily used to simulate the condition in which heterogeneous nucleation competes most favorably. Note that model S, using the particle tracing scheme, records the evolution of a total of 20000 particles, or a parcel of volume 100 cm^3 at the starting point of simulation. Therefore, its minimum detectable change in ice number concentration is $\sim$0.01 cm^{-3}.

c. Haze particle size and solution concentration

There are differences in the specification of haze size and solute wt% (Table 2). These differences may significantly affect model results, e.g., nucleation triggering humidity, ice particle formation rate, and freezing haze distributions.

The volume of a haze particle is given by

$$V = m_s \frac{1 + \frac{1000}{M_s \mathcal{M}}}{\rho_s(\mathcal{M})} \tag{10}$$

where $\mathcal{M}$, m_s, and ρ_s are molality (mol of solute per 1000 g of water), solute mass, and solution density, respectively, in C. G. S. units. Within the temperature and moisture ranges considered in this study, the volume of equilibrium-sized haze particles of a given solute mass varies within a factor of 10. Following Eq. 10 and Fig. 2, the sensitivity of $J_{haze}V$ to haze volume is far less than to solution molality, temperature, and λ. However, if haze radius is the prognostic or diagnostic variable in a model, and the water mass of haze is derived by $m_w = \rho_s V - m_s$, solution density is not a trivial issue. The difference in ρ_s would significantly affect the obtained solute wt%. Measurements of the H_2SO_4 solution density for temperature below 0°C were not available until the work by Myhre et al. (1998). They showed that extrapolation of existing ρ_s data which were measured above 0°C matches well with their measurements. Participants of this project used different formulae for solution density, explicitly or implicitly (Fig. 4). We suggest that solution density, in future studies, be specified with care.

Haze particles are in equilibrium with the environment except (i) when temperature is greater than -42°C and the required RH_w to trigger homogeneous nucleation is close to, or greater than, unity (Heymsfield and Sabin 1989); and (ii) in a strong updraft associated with a cold environment (to be discussed more in the following). When equilibrium is assured, the haze particle size can be obtained by iteration either using (e.g. models D

and L[2]):

$$S_w = a_w \exp(\frac{2\sigma_{s/a}}{\rho_w R_v T r}), \tag{11}$$

where $a_w = \exp(-\frac{\nu \Phi_s m_s M_w}{m_w M_s})$, or the dilute solution approximation ($\ln S_w \approx S_w - 1$; $\Phi_s \approx 1$; $m_w >> m_s$; $\rho_s \approx \rho_w$, e.g. models C and S[3]):

$$S_w - 1 = -\frac{3\nu(M_s/M_w)m_s}{4\pi\rho_w r^3} + \frac{2\sigma_{s/a}}{\rho_w R_v T r}. \tag{12}$$

If using a temperature-independent a_w formula (Chen 1994), the haze equilibrium radius is not very sensitive to temperature within the cirrus temperature range (-45 to -65 °C) considered in this project, especially for haze with solute mass greater than 10^{-15} g. In other words, Kelvin's effect (or the curvature effect) is controlled by the value of solute mass and is not sensitive to a 10% change in either temperature nor haze surface tension $\sigma_{s/a}$ within this temperature range. If using a temperature-dependent a_w formula (Clegg and Brimblecombe 1995), the required S_w for the equilibrium condition fluctuates within ± 0.005 in this temperature range. This temperature and molality dependent water activity is adopted by models D and J.

Figure 5 compares solute wt% computed by models C (Eq. 12) and L (Eq. 11) as the solid and dashed lines, respectively. The obtained equilibrium haze solute wt% by model C can be a few percent lower (higher) than that obtained by model L in the high (low) ambient humidity RH_w condition. Note that substantial differences in solute wt%

---

[2]Model L used fitted functions based on (11).

[3]Model S uses equation (50) of Fukuta and Walter (1970) to compute the equilibrium haze radius. Yet, the model sets $\Phi_s = 1$, $\nu = 3$. Model S renders equilibrium haze solute wt% close to that of model C, which also sets $\nu = 3$, when solution is dilute.

exist even at $RH_w \sim 95\%$, probably because the assumption that $\Phi_s = 1$, $\nu = 3$ in the dilute approximation deviates significantly from the a_w used by models D and L. Curves of equilibrium haze volume for the two approaches gradually become divergent as RH_w decreases.

The equilibrium haze solute wt% by model S coincides with those of model C when humidity is high. However, they deviate from model C as humidity decreases. This trend results from the differences in solution density specification in the two models and demonstrates the importance of ρ_s when acquiring equilibrium solution concentration from haze radius. This result has obvious consequences on $\lambda \Delta T_m$ and thus nucleation rate. In the cases that haze particles are approximately in equilibrium with the environment (will be discussed further in the Section 4a1), Fig. 5 may provide useful information about the nucleation triggering RH_w.

Multi-dimensional models cannot afford to iterate. Thus, further simplification is required for parcel models which are modules of multi-dimensional models. Model L uses fitted functions based on Eq. 11. Model J neglects Kelvin's effect and sets $a_w = S_w$, for which the equilibrium haze solute wt% becomes only a function of environment S_w. As shown in Fig 5, Kelvin's effect results in 1 to 2% solute wt% differences between haze containing solute 10^{-15} and 10^{-12}g. This is a significant difference (Fig. 2). Hence, ignoring Kelvin's effect enhances the freezing possibility of particles with small solute mass and leads to the broadening of the freezing haze particle size distribution.

The equation for diffusional growth of haze particles is given by (Fukuta and Walter 1970)

$$\frac{dm_w}{dt} = \frac{4\pi r(S_w - S_w^*)}{\frac{R_v T}{e_{s,w} D'} + (\frac{L_v}{R_v T} - 1)\frac{L_v}{TK'} S_w^*}, \tag{13}$$

where S_w^* is obtained by substituting the instantaneous haze radius and solute wt% into Eqs. (11) or (12) depending on the models. The heat transfer contribution term (the second term in the denominator) is more than an order of magnitude smaller than the mass transfer term (the first term in the denominator) in the temperature range considered here. Thus, the following discussion focuses only on the effect of the mass transfer term and its sensitivity to condensation coefficient, β_w. The diffusional growth rate decreases exponentially with temperature and reflects the strong temperature dependence of saturation water vapor pressure. The response time scale to the deviation from equilibrium can be considerably greater than one model time step in a cold environment. The stronger the updraft, the wider the gap between these two time scales may be. Therefore, haze with high solute mass become more concentrated than the corresponding equilibrium-size particles in a cold environment and strong updraft conditions.

Haze particle growth rate is sensitive to β_w, which modifies the value of D' and has to be included with caution. Both models C and S use $\beta_w = 0.05$ resulting in considerable delaying of haze growth in several simulations. In contrast, diffusional growth of haze particles does not cause noticeable effects on haze solute wt% in simulations by model L because a much higher β_w is used.

Figure 6 shows haze solute wt% with respect to solute mass by model C just before homogeneous nucleation is triggered. Large haze particles deviate from the equilibrium condition (approximately the 0.04 m s^{-1}) as the strength of updraft increases. The haze particles that are most dilute are not necessarily the largest ones when the limit of diffusional growth is imposed (e.g., the Ch100 curve). In comparison, the deviation from equilibrium is not as significant in the warm cases. Haze solution concentration is close

to being in equilibrium with the environment in the slow and moderate updraft cases (Wh004 and Wh020). Note that ±1% in wt% at wt% = 20% results in approximately a 3°C difference in T_{eff} when $\lambda = 2$ (Fig. 3).

4. Model results and discussion

A parcel lifted by an updraft goes through four stages (Fig. 7). In the first stage, the parcel cools adiabatically and expands. Haze particles grow, but uptake of vapor by these particles is negligible.

The nucleation regime starts as the first ice crystals form. We arbitrarily define the level at which ice particle number concentration N_i reaches 1 L^{-1} as the beginning of the nucleation regime or cirrus cloud base z_b (relative to the parcel initial height z_{ini}). Ice water content (IWC) and N_i increases afterwards. In the beginning of this stage, RH_i tendency ($\frac{dRH_i}{dt}$) is positive but decreasing in magnitude due to vapor uptake by growing ice crystals. Homogeneous nucleation, if activated, shuts off shortly after RH_i reaches its peak value. The homogeneous nucleation regime takes place within relatively a small range of vertical displacement of the parcel.

The next regime features a rapid decrease in RH_i corresponding to the rapid increase of IWC. RH_i tendency starts from 0, falls to a minimum, then increases asymptotically to zero. The equilibrium regime begins when $\frac{dRH_i}{dt} \sim 0$. In general, the parcel's temperature tendency $\frac{dT}{dt}$ is close to ice moist-adiabatic in the equilibrium regime, although this may depend on the value of RH_i at equilibrium (hereafter, $RH_{i,eq}$).

Comparison of N_i generated by the different models is the center piece of this project (Fig. 8). Note that N_i at 800 m, where little additional nucleation is occurring, above

z_{ini} is compared. Temperature differences among models at this level are negligible. In the HN-ONLY cases, to a first order approximation, the logarithm of ice crystal number concentration increases quasi-linearly with the logarithm of updraft speed. Increase of N_i with W was first demonstrated by Heymsfield and Sabin (1989) and Sassen and Dodd (1989) and followed by others. This figure demonstrates that while all models manifest this trend of N_i with W, the quantitative differences among models can not be overlooked and have to be studied in detail. The predicted N_i by models D, S and L are close. The predicted N_i by models J and C tend to form the lowest and highest bounds in the six cases, respectively. The difference in N_i among the models reach as large as a factor of 25. Comparing the predicted N_i in these two temperature regimes, generally speaking, more ice crystals are generated in the cold cases. This tendency was also first reported by the aforementioned pioneer works. Jensen and Toon (1994) conjectured that the inverse trend of ice crystal growth rate with temperature was the primary cause.

The cloud base RH_i, z_b and ΔRH_i (peak RH_i minus RH_i at z_b) increase with the updraft speed in the HN-ONLY cases (Fig. 9). Cirrus forms in a narrower range of altitude in the warm cases ($360 < z_b < 400$m, Fig. 9b) than in the cold cases ($325 < z_b < 410$m, Fig. 9a). Following the research of Lin et al. (1998) on cloud properties sensitivity in lift-limited situations, if the depth of updraft region is incidentally between the minimum cloud base height and the maximum nucleation-ceasing altitude of all models, the discrepancy in the predicted N_i would be greatly enhanced.

The corresponding range of cloud base RH_i in the warm cases is also smaller than that in the cold cases. The primary factor of the increasing sensitivity of the cloud base RH_i as temperature decreases in the four T_{eff}-approach models has been discussed in

section 3a: the range of critical freezing RH_w corresponding to a given range of λ increases with the decrease of ambient temperature. Generally speaking, smaller λ entails lower cloud base height. Other factors (e.g. differences in solution density, specification of haze particle solution concentration, saturation water vapor pressure over water) may also affect the cloud base RH_i. This is why in the cold cases, models C and D using $\lambda = 1.5$ obtain different cloud base RH_i, and in the warm cases the sequence of the time that nucleation is triggered does not follow the values of λ.

The cloud base RH_i, z_b, and peak RH_i in the ALL-MODE cases vary even more because of our respective unbounded choices of heterogeneous nucleation (Fig. 10). The impact of heterogeneous nucleation on lowering N_i, peak RH_i, and cloud formation altitude is extremely sensitive to the onset conditions for nucleation and the subsequent rate of ice formation. Switching on heterogeneous nucleation, the peak RH_i is lower in all but the case Wa100 by model S, possibly because of the height dependency in ice nuclei concentration. The predicted N_i is reduced in all but the case Ca004 by model S, which will be discussed further below.

Here we define the N_i reduction ratio as the N_i of the ALL-MODE case over that of the corresponding HN-ONLY case (Table 3). The small N_i reduction ratio in models C and L may be traced to their sensitivity to S_i that is not mitigated by any attachment to aerosol number concentration or size and the low RH_i onset condition for heterogeneous nucleation (e.g., $S_i > 1$ in model L). The difference of N_i between ALL-MODE and HN-ONLY cases by model D is only prominent in the warm and slow updraft case (Wa004). The weak influence of heterogeneous nucleation in model D is tied to two factors. First, the maximum IN concentration predicted by the formulation are no more

than a few hundred per liter in the range of conditions simulated. Secondly, the lowering of the onset RH_i for ice formation is limited by solute concentration via the use of effective freezing temperature in the immersion freezing mechanism.

The N_i reduction ratios of model S are significantly higher at the 0.04 m s^{-1} cases. The predicted N_i in Ca004 is even larger than that of Ch004; N_i of Ca004 increases exponentially with height from 200 m above the starting level (not shown). It is possible that the anomaly behavior for this single model run results from the large value of B_s used. However, this large B_s is the only value capable of producing significant heterogeneous nucleation, in view of the height-dependent term in Eq. 9. More study is required to understand this anomaly.

Recent model intercomparison projects demonstrate that the benchmark is not necessarily the median or the average of model results. With this in mind, we investigate the reasons causing the noted differences, emphasizing the HN-ONLY simulations.

a. Causes of variability in the λ-fixed simulations

The number density of haze particles freezing in time interval Δt is formulated as

$$\frac{dN_i}{dt}\Delta t = \sum_k N_{haze,k}(t)[1 - \exp(-J_{haze,k}V_k\Delta t)], \tag{14}$$

where the summation in k is the integration over haze particle size bins, and $\frac{dN_i}{dt}$ is termed as ice particle formation rate afterwards. It can be shown that the predicted ice particle number density is simply

$$N_i = \sum_k N_{haze,k}(t=0)(1 - \exp(-\int_0^t J_{haze,k}V_k dt)). \tag{15}$$

Factors of a hierarchy interact with each other to result in the difference in the

predicted N_i. Given temperature, size and solute wt% of a haze particle, the difference in formulating the homogeneous freezing nucleation would affect the nucleation rate on one single haze particle level. Haze particle specification and evolution, together with homogeneous freezing nucleation formulation, determine the the instantaneous ice particle formation rate. Given an uplift speed, the diffusional growth rate of ice crystals in combination with all of the above components control the water vapor uptake rate, and thus the evolution of the parcel RH_w, which then determines the predicted N_i. The results of the λ-fixed simulations are examined to understand these interactions and feedback in depth.

1). The level at which homogeneous nucleation is triggered

We now discuss the results of the simulations for which participants set the coefficient $\lambda = 2$ (or an approximation of this in model J). These simulations (Ch020L and Wh020L) sought to minimize differences in predicted nucleation rates as a source of discrepancies in the results. It was found that the nucleation regimes of participant models occurred within the temperature range of -43.2 to -44.2°C and -63.2 to -64.2°C in the two simulations. The effect of temperature variation on nucleation rates within this 1°C range is secondary compared to the evolution of RH_w. Therefore, it is justified to analyze model results according to the $z - z_b$ level. The results of this analysis are shown in Fig. 11.

The range of triggering RH_w was reduced as expected to less than 2% in Wh020L and 5% in Ch020L in comparison to 3% and 8% in simulations Wh020 and Ch020. Note that participants use different formulae to compute saturation vapor pressure over water and ice. These formulae gradually diverge as temperature becomes lower than -45°C so we

use RH_w here. Its effects on predicted N_i will be further explored in the Phase 2 of this project.

There are still significant differences in N_i among the models. It can be seen that N_i is only slightly changed by the value of λ when comparing N_i of cases $\lambda = 2$ with the corresponding λ-unspecified cases. In the cold cases, the increase in λ results in a slight decrease in the predicted N_i in models D and L whereas the predicted N_i by models C and S are not much affected. Contrarily, in the warm cases, the increase in λ results in a slight increase in N_i in the four models of the T_{eff} approach family. Additional study of the effect of λ is planned in Phase 2 of this project. In the light of these results, λ is not the dominant factor controlling the number concentration of ice crystals nucleated.

In Wh020L, haze particles are almost in equilibrium with the environment. Nucleation is triggered at around $RH_w = 95.5\%$ in models C, J and S, suggesting that aerosols with solute wt% around 8-9% in models C and S and 11% in model J start to freeze at this condition (Fig. 5). As shown in Fig. 5, in models D and L, the equilibrium-sized aerosols of solute wt% 8$\sim$9% are not formed until ambient RH_w is around 97%. This is probably the reason why the nucleation triggering RH_w by models C and S is about 1% lower than those of models D and L.

Compared with Wh020L, the order of nucleation triggering RH_w in Ch020L switches among the four models using T_{eff} approach. Models D and L have the lowest nucleation triggering RH_w in this case. As shown in Fig. 5, if models S and C turn off diffusional growth of haze particles and use equilibrium-sized particles instead, models S and C would have a lower or similar triggering RH_w than those of models D and L, respectively. It is suspected that the diffusional growth of haze particles may delay the nucleation being

triggered.

2). The nucleation regime

At the beginning of the nucleation stage in simulation Wh020L, ice particle formation rates are close among the four models of the T_{eff} approach group (Fig. 11). However, models C and D reach much higher RH_w that leads to higher instantaneous nucleation rates, and maintain the peak ice formation rate longer than the other two models. The ranges between RH_w at z_b and peak RH_w thus are higher in these two models. As a consequence, model C has the highest N_i followed by model D.

The curve grouping of ice particle formation rates in simulation Ch020L are not exactly the same as those in Wh020L. From the start of the nucleation stage in this simulation, the N_i curves of models D and L distinctly separate from those of models C and S. This grouping incidentally coincides with the grouping according to the haze particle specifications. Haze particles are in equilibrium or close to equilibrium in models D and L while large haze particles are more concentrated than the corresponding equilibrium values in models C and S. The ice particle formation rates in models C and S are more than one order greater than those by models D and L. Yet, the nucleation regime in model S does not sustain as long as in model C; a similar observation is noted when comparing results of model D and L. Near the end of the nucleation regime, model C has the highest N_i. Model S has slightly larger N_i than model D, despite the fact that the former has a much higher initial ice particle formation rate. The long nucleation duration in model D eventually produces a value of N_i that is comparable to model S. The reason for these discrepancies among T_{eff} group is a complicated combination of differences

in haze specification (discussed in this paragraph), deposition coefficient, and numerical procedures (to be discussed in this section later).

The ice particle formation rate by model J is smaller than the rest. The range of RH_w between z_b and peak is also wider in simulations by model J. From Fig. 12, the freezing haze number distribution in simulations by model J is much broader. These three distinct features of model J might result from a combination of the following elements. The homogeneous nucleation scheme of model J is less sensitive to solution concentration compared to the others; the curvature effect is ignored when computing haze size; and with ice particle formation rate an order of magnitude smaller than the others, and with the long nucleation duration, the average size of ice crystals in model J can be much greater when nucleation stops.

To a first order approximation, the logarithm of ice particle formation rate is parabolically centered at peak $\frac{dN_i}{dt}$ (Fig. 11), suggesting that the curve of ice particle formation rate along the z axis can be approximated by a normal distribution. Therefore, the ice crystals nucleated $N_i = \int_0^t \frac{dN_i}{dt} dt$ can be approximated as $N_i = \sqrt{\frac{\pi}{2}} \frac{dN_i}{dt}|_p \Delta t$, where Δt is the width of the curve and $\frac{dN_i}{dt}|_p$ is the peak value of ice particle formation rate. The evolution of ice water content, which is the cumulative water vapor uptake, as aforementioned, will control the peak RH_w and $\frac{dN_i}{dt}|_p$. The vapor uptake rate at any instance is equal to the summation of ice crystal growth rate times N_i. The growth rate of small ice crystals ($r < 10\mu$m), under the influence of the kinetic effect, is quite sensitive to the deposition coefficient β_i. Sensitivity tests on β_i have been performed to check its effect in isolation. It is found by both models D and L that varying β_i from 0.04 to 1, the range of β_i values specified by participants (Table 2), would result in about a factor of 4~5

and 9~12 variation in the predicted N_i in Wh020L and Ch020L, respectively (Fig. 13). Nucleation begins at the same RH_w, but simulations with small β_i reaches high RH_w and trigger freezing of many small haze particles. The predicted N_i decreases as β_i increases from 0.04 to 0.2; it only adjusts marginally to β_i when $0.2 < \beta_i < 1$. It is worth noting that by adjusting β_i alone, model D was able to obtain N_i predicted by model J.

A systematic bias in N_i and IWC relationships among models is prominent (Fig.14). At a given N_i level, model C uptook the least amount of water vapor while model J the most. Eventually, model C (J) stopped producing ice particles at much higher (lower) N_i compared with other models. The mismatch between β_i values and the N_i and IWC bias suggests that the difference in β_i is a crucial but not the only component to result in this systematic bias. It is conjectured that an intrinsic characteristic of the numerical component, e.g., bin characteristic, would also affect the ensemble growth rate. By increasing the frequency to rebin ice particle size distribution (every 5 m to every 0.5 s), the predicted N_i of model C is significantly reduced. Results after revision by model C will be discussed more in the forthcoming paper about Phase 2 of CPMC.

b. All-mode simulations versus homogeneous-nucleation-only simulations

Heterogeneous nucleation is a possible explanation for the discrepancy between the observed threshold RH_w required for cirrus formation and the theoretically derived threshold RH_w to trigger homogeneous nucleation in H_2SO_4 or $(NH_4)_2SO_4$ solution particles (Heymsfield and Miloshevich 1995; DeMott et al. 1997). Cirrus microphysical and radiative properties are affected by the dominant nucleation mode in cloud initiation because ice particle formation rates of the two modes are expected to be distinct. First of

all, the threshold humidity for heterogeneous nucleation of ice in a water-subsaturated and ice-supersaturated environment may be much less than that for homogeneous nucleation. If the upward motion is confined within a thin layer, in which the maximum humidity that may be achieved by an ascending parcel is between the threshold humidity of the two modes, the presence of IN will determine if cirrus forms or not. If the vertical displacement of parcels is big enough to provide the necessary condition to trigger homogeneous nucleation, the presence of IN may partially or completely suppress homogeneous nucleation and change the cloud properties depending on ice nuclei characteristics (Sassen and Benson 2000). Generally speaking, the biggest difference in N_i between the ALL-MODE and HN-ONLY simulations takes place when the updraft speed is slow to moderate and homogeneous nucleation is completely suppressed (Fig. 8 and Table 3). Complete suppression of homogeneous nucleation is achieved when the uptake of excess water vapor by ice crystals formed by heterogeneous nucleation sufficiently lowers the maximum humidity achieved by the parcel. Hence for a given cooling rate, a larger difference between the threshold humidity of the two modes would provide particles more time to grow and thus a more favorable condition for suppression. Of all ALL-MODE simulations by model D, homogeneous nucleation is completely suppressed only in case Wa004. It is found that the difference of threshold humidity of the two modes in model D is the smallest. This directly relates to the conservative estimate of the concentrations of available heterogeneous ice nuclei (as a function of T and RH) made in model D.

Information about detailed ice crystal size distributions enables us to compute the

volume absorption coefficient of b_{abs} as

$$b_{abs} = \sum_k Q_{abs,k} \pi r_k^2 N_{ice,k}, \tag{16}$$

where Q_{abs} is the absorption efficiency obtained from Mie theory assuming spherical ice particles. The absorption efficiency at wavelength 10.75 μm increases from 0.27 for ice particles $r = 1\mu$m to 1.12 for particles $r \sim 15\mu$m, and gradually decreases to ~ 1.0 as particles radius equals 250 μm.

From Fig. 15, on average, the absorption coefficient increases with updraft speed. The difference in absorption coefficient among models in the HN-ONLY simulations can be more than 100%. Except for simulation Ca100 by models C and S, b_{abs} of HN-ONLY cases is higher than that of their ALL-MODE counterparts; maximum differences exceeding 100% are found between ALL-MODE and HN-ONLY simulations. Though the uncertainty of estimated ice crystal number concentration is 25-fold in the extreme, the uncertainty of estimated optical properties is about twofold for a given cooling rate.

Ice crystal size distribution information also gives us a unique chance to check the calculation of cloud optical properties using effective radius. Current parameterization of cloud optical properties usually incorporates b_{abs} in the form

$$b_{abs} = \kappa(d_e) IWC, \tag{17}$$

where κ and d_e are the mass absorption coefficient and the effective length of the ice crystal distributions, respectively (e.g., Ebert and Curry 1992; Fu et al. 1998). In Fig. 15, r_e is computed according to $r_e = \frac{\sum_k r_k^3 N_k}{\sum_k r_k^2 N_k}$ (Ebert and Curry 1992). We do not have to worry about the definition of r_e used because in our simple simulations assuming spherical particles, all types of definition of d_e converge (McFarquhar and Heymsfield 1998). Note

that the mass absorption coefficient decreases as effective radius increases only in the range of r_e greater than $\sim$20 μm.

The maximum difference in IWC among models for the cold or the warm cases is less than 15%. It is evident that the difference in IWC can not explain the large difference in b_{abs} for two simulations with similar r_e. The effective radii of case Ch020 obtained by models D and S are about the same. However, b_{abs} of the two models calculated according to Eq. 16 shows significant difference. We found that the ice crystal distribution by model D is much broader than that by model S in this case.

The difference of N_i between ALL-MODE and HN-ONLY is the least when W = 1 m s^{-1}. However, except for model D, b_{abs} in cases Ch100 and Ca100 for all models are close unlike the values of b_{abs} in cases Wh100 and Wa100 (Fig. 15). We speculate that the growth rate difference in these two temperature regions is the major factor. The growth rates of ice crystals in the warm cases are much higher than those in the cold cases. As a consequence, ice crystal distributions in Wa100 are considerably broader than their corresponding Wh100 simulations. This is not so in the cold cases.

The mass weighted terminal velocity $V_t = \frac{\sum_k V_{t,k} m_k N_k}{IWC}$ is also plotted in Fig. 15. As far as ice mass flux is concerned, the model-to-model differences in V_t are negligible in the W = 1 m s^{-1} cases. Ice mass flux is weighted favorably to the amount of large particles. Percentage-wise, the resultant difference in ice mass flux between HN-ONLY and ALL-MODE cases is bigger than that in b_{abs}.

The RH$_{i,eq}$ (see Section 4) of parcel models provides GCM and cirrus models, which use a moisture-adjustment scheme to convert excess water vapor to cloud ice mass (e.g., Starr and Cox, 1985; Krueger et al., 1995), with a guideline to set the threshold RH$_i$. It

can be shown that the $RH_{i,eq}$ is proportional to W and inversely related to N_i. Figure 16 demonstrates the relation between these three components at 800 m above the starting point of the simulations. The $RH_{i,eq}$ is well within 110% except for cases Wa020 and Ca020 by model L. However, the moisture-adjustment time scale, the time interval between the peak RH_i and $RH_{i,eq}$, also has to be considered to render a complete view. Note the moisture-adjustment time scale defined in this paper is conceptually similar to the phase relaxation time defined in Khvorostyanov and Sassen (1998a), yet it differs from the phase relaxation time because the latter is defined according to the local gradient. The moisture-adjustment time almost decreases exponentially with updraft speed. For example, at W = 0.04, 0.2, 1 m s^{-1}, the time scales are roughly 30 $\sim$ 100 min, 6 $\sim$ 40 min and 1 $\sim$ 6 min, respectively (Fig. 15). Therefore, RH_i higher than 110% can be frequently detected in regions of small to moderate cooling rates. This suggests that models using time steps of around 1-hr may set a nucleation RH_i and a threshold RH_i to simulate cold cirrus in a weak (synoptic) ascent; models using smaller time steps face a more difficult modification.

5. Summary

Broad qualitative agreement has been found in the simulations wherein homogeneous nucleation was the only nucleation mechanism activated. The model predicted cirrus microphysical and optical properties are strongly influenced by the updraft speed. However, significant differences were found in the predicted ice crystal number concentrations N_i and ice crystal size distributions. For a given cooling rate, there was up to a factor of 25 difference in N_i, for the conditions simulated, resulting in factors of 2 to 3 differences in

infrared absorption coefficient and ice mass flux at the end of simulation (800 m above the starting point of the parcel ascent).

Detailed examination of the output of HN-λ-fixed simulations revealed that the homogeneous nucleation formulation, haze particle solution concentration, and ice crystal growth rate were critical factors to affect the water vapor uptake rate, the peak ice supersaturation the parcel achieved, and, subsequently, the predicted N_i. Our chief findings can be summarized as follows:

- The parameter λ mainly affects the required initiation humidity to trigger homogeneous nucleation. Preliminary results show that the predicted N_i is marginally affected by a reasonable choice of λ.

- Ignoring Kelvin's effect would result in the broadening of the freezing haze size distribution, which represents an enhancement of the model sensitivity to the existence of small haze particles. It is also found that the modified classical scheme produces broader freezing haze size distributions than the T_{eff} approach.

- The equilibrium assumption of haze particle size is violated in strong updrafts in a cold environment. Assuming equilibrium may result in underestimate of ice particle formation rate at the beginning of the cloud initiation stage.

- The condensation/evaporation coefficient for ice, which directly affects the growth rate of small ice crystals, is a critical factor determining the predicted N_i.

Disagreement in formulating the homogeneous nucleation of condensed solution particles by the T_{eff} approach and the classical approach indicates that the critical freezing

condition measured in laboratory work provides only a part of information necessary to construct a consistent way to formulate the homogeneous nucleation rate. These results highlight the need for new laboratory and field measurements to infer the correct values for the critical quantities in the cirrus regime.

In general, discrepancies among models were greater in the ALL-MODE simulations. No attempt was made to scrutinize the causes of differences in ALL-MODE simulations due to lack of strict restriction to formulate heterogeneous nucleation. Nevertheless, it was confirmed that the expected effect of a heterogeneous nucleation process is to lower N_i and the RH_i required for cloud initiation, and increase the average size of ice crystals formed in cirrus clouds compared to the case of a singular homogeneous freezing process. Clearly, new measurements of ice nuclei activation in cirrus conditions are warranted. Moreover, it is important to come to grasp with the effects of solution droplet strength and chemistry on the activation of ice nuclei.

This study was conducted based on a single CCN distribution. The sensitivity of predicted cirrus microphysical and optical properties to the assumed CCN distribution must be addressed in order to advance this study. In Phase 2 of the CPMC, now underway, the effects of varying input aerosol distributions (e.g., number concentration, mode radius, and distribution width) are taken into account. Sensitivity of model results to CCN composition will indirectly be made by altering the value of λ.

Notation

A Coefficient in the heterogeneous nucleation scheme used by model C [2.7×10^{10} m^{-3}]

A_{s0} Coefficient in the modified Fletcher eq. used by model S [10^{-2} m^{-3}]

A_z Coefficient in the modified Fletcher eq. used by model S [7.5×10^{-4} m^{-1}]

a Coefficient in the immersion freezing parameterization by model D [1.3×10^{-23}, dimensionless]

a_w Water activity

B Coefficient in the heterogeneous nucleation scheme used by model C [10.6, dimensionless]

B_s Coefficient in the modified Fletcher eq. used by model S [0.8 $°C^{-1}$]

b Coefficient in the immersion freezing parameterization by model D [11.75, dimensionless]

b_{abs} Volume absorption coefficient [m^{-1}]

B_z Boltzmann constant

C_p Specific heat capacity for dry air at constant pressure [J kg^{-1} K^{-1}]

d_e Effective length for a distribution of particles for optical properties calculation [m]

D' Coefficient of diffusion of water vapor in air modified by kinetic effect (See Eq. (13-14) of (Pruppacher and Klett 1997)) [m^2s^{-1}]

$e_{s,w}$ Saturation water vapor pressure over a flat pure water surface [Pa]

F_k Number fraction of haze particles frozen in bin k

ΔF_{actv} Activation energy for diffusion of a water molecule across the water-ice boundary [J]

ΔF_{germ} Energy of ice-germ formation [J]

$F_{>0.1\mu m}$ CCN fraction of haze size greater than 0.1 μm

g Acceleration due to gravity

h Planck constant

IWC Ice water content [kg m^{-3}]

J_w Homogeneous nucleation rate of ice in pure water [m^{-3} s^{-1}]

J_{haze} Homogeneous nucleation rate of ice in solution droplet [m^{-3} s^{-1}]

K' Coefficient of diffusion of water vapor in air modified by kinetic effect (See Eq. (13-20) of (Pruppacher and Klett 1997)) [J m^{-1} s^{-1} K^{-1}]

$\overline{L_m}$ Average latent heat of fusion of water between T and T_0 [J kg^{-1}]

L_v Latent heat of condensation [J kg^{-1}]

$\mathcal{M}$ Molality [mol per 1000 g of water]

M_s Molecular weight of solute

M_w Molecular weight of water

m_s Solute mass

m_w Water mass

N_c Number of monomers of water in contact with unit area of the ice surface [m^{-2}]

$N_{haze,k}$ Number concentration of haze particles in bin k [m^{-3}]

N_i Number concentration of ice crystals (total) [m^{-3}]

$N_{ice,k}$ Number concentration of ice crystals in bin k [m^{-3}]

N_{IN} Number concentration of activated ice nuclei [m^{-3}]

P Pressure [Pa]

Q_{abs} Absorption efficiency

$\dot{Q}_{LH}$ Diabatic heating due to latent heat release [K s^{-1}]

R_d Gas constant for dry air [J kg^{-1} K^{-1}]

R_v Gas constant for water vapor [J kg^{-1} K^{-1}]

RH_i Relative humidity wrt. ice

RH_w Relative humidity wrt. water

r Radius [m]

r_e Effective radius for optical properties [m]

S_i Water vapor saturation ratio wrt. ice

S_w Water vapor saturation ratio wrt. water

T Temperature [K]

T_0 Reference temperature 273.15 K

T_{eff} Effective freezing temperature [K]

ΔT_m Melting point depression [K]

t Time [s]

Δt Time interval [s]

V Volume [m^3]

V_t Terminal velocity [m s^{-1}]

W Updraft speed [m s^{-1}]

z Height [m]

z_b Height at which ice number concentration becomes 1 L^{-1} [m]

α Coefficient in the heterogeneous nucleation scheme used by model L [7.5468, dimensionless]

β Coefficient in the heterogeneous nucleation scheme used by model L [0.1296, dimensionless]

β_i Deposition coefficient

β_w Condensation coefficient

λ See section 3.

Γ Lapse rate [K m^{-1}]

ρ_i Ice density [kg m^{-3}]

$\overline{\rho_i}$ Average ice density between T and T_0[kg m^{-3}]

ρ_s Solution density [kg m^{-3}]

ρ_w Water density [kg m^{-3}]

$\sigma_{a/s}$ Surface tension across the air and solution interface [J m^{-2}]

$\sigma_{i/s}$ Surface tension across the ice and solution interface [J m^{-2}]

ν Dissociation constant for ions in solution

Φ_s Molal osmotic coefficient

Subscripts *eq*, *ini*, k and p denote equilibrium, the initial condition, category k and the peak value, respectively.

Acknowledgments.

The U.S. DOE ARM Program and NASA Radiation Sciences Program have provided direct support (RFL and DS) for this GCSS project. We thank support from UK Met. Office (RC), NSF-ATM9632917 (PJD), NASA's Stratospheric Aerosol and Gas Experiment (EJ), NSF-ATM9528287 (KS) and DOE grant DEFG0394ER61747 (KS). K. Sassen also thanks S. Benson and Z. Wang for their help.

References

Chen, J.-P., 1994: Theory of deliquescence and modified Köhler curves, *J. Atmos. Sci.*, **51**, 3505-3516.

Chen, J.-P., and D. Lamb, 1994: Simulations of cloud microphysical and chemical processes using a multicomponent framework. Part I: Description of the microphysical model, *J. Atmos. Sci.*, **51**, 3505-3516, 1994.

Chen, Y., P. J. DeMott, S. M. Kreidenweis, D. C. Rogers, and D. E. Sherman, 2000: Ice formation by sulfate and sulfuric acid aerosol particles under upper tropospheric conditions, *J. Atmos. Sci.*, **57**, 3752-3766.

Clegg, S. L., and P. Brimblecombe, 1995: Application of a multicomponent thermodynamic model to activities and thermal properties of 0-40 mol kg^{-1} aqueous sulfuric acid from <200 to 328 K, *J. Chem. Eng. Data*, **40**, 43.

Colella, P., and P. R. Woodward, 1984: The piecewise parabolic method (PPM) for gas-dynamical simulations, *J. Comput. Phys.*, **40**, 174-201.

Darlison, A. G., 1988: Modelling the initial ice crystal spectrum in cirrus cloud, *Proc. 10th Int. Conf. Cloud Physics*, Bad Hömburg, 485-487.

DeMott, P. J., and D. C. Rogers, 1990: Freezing nucleation rates of dilute solution droplets between -30° and -40°C in laboratory simulations of natural clouds, *J. Atmos. Sci.*, **47**, 1056-1064.

DeMott, P. J., M. P. Meyers, and W. R. Cotton, 1994: Parameterization and impact of ice initiation processes relevant to numerical model simulations of cirrus clouds, *J. Atmos. Sci.*, **51**, 77-90.

DeMott, P. J., D. C. Rogers, and S. M. Kreidenweis, 1997: The susceptibility of ice formation

in upper tropospheric clouds to insoluble aerosol components, *J. Geophys. Res.*, **102**, 19,575-19,584.

DeMott, P. J., D. C. Rogers, S. M. Kreidenweis, Y. Chen, C. H. Twohy, D. Baumgardner, A. J. Heymsfield, and K. R. Chan, 1998: The role of heterogeneous freezing nucleation in upper tropospheric clouds: Inferences from SUCCESS, *Geophys. Res. Lett.*, **25**, 1387-1390.

DeMott, P. J., 2001: Laboratory studies of cirrus cloud processes, in *Cirrus*, edited by D. K. Lynch, K. Sassen, and D. O'C. Starr, Oxford University Press, London (in press).

Ebert, E. E., and J. A. Curry, 1992: A parameterization of ice cloud optical properties for climate models, *J. Geophys. Res.*, **97**, 3831-3836.

Fu, Q., P. Yang, and W. B. Sun, 1998: An accurate parameterization of the infrared radiative properties of cirrus clouds for climate models, *J. Climate*, **11**, 2223-2237.

Fukuta, N., and L. A. Walter, 1970: Kinetics of hydrometeor growth from a vapor-spherical model, *J. Atmos. Sci.*, **27**, 1160-1172.

Gierens, K., and E. J. Jensen, 1998: A numerical study of the contrail-to-cirrus transition, *Geophys. Res. Lett.*, **25**, 4341-4344.

Heymsfield, A. J., and L. M. Miloshevich, 1993: Homogeneous ice nucleation and supercooled liquid water in orographic wave clouds, *J. Atmos. Sci.*, **50**, 2335-2353.

Heymsfield, A. J., and L. M. Miloshevich, 1995: Relative humidity and temperature influences on cirrus formation and evolution: Observations from wave clouds and FIRE II, *J. Atmos. Sci.*, **52**, 4302-4326.

Heymsfield, A. J., and R. M. Sabin, 1989: Cirrus crystal nucleation by homogeneous freezing of solution droplets, *J. Atmos. Sci.*, **46**, 2252-2264.

Heymsfield, A. J., L. M. Miloshevich, C. Twohy, G. Sachse, and S. Oltmans, 1998: Upper-

tropospheric relative humidity observations and implications for cirrus ice nucleation, *Geophys. Res. Lett.*, **25**, 1343-1346.

Howell, W. E., 1948: The growth of cloud drops in uniformly cooled air, *J. of Met.*, **6**, 134-149.

Jeffery, C. A., and P. H. Austin, 1997: Homogeneous nucleation of supercooled water: results from a new equation of state, *J. Geophys. Res.*, **102**, 25,269-25,279.

Jensen, E. J., and O. B. Toon, 1992: The potential effects of volcanic aerosols on cirrus cloud microphysics, *Geophys. Res. Lett.*, **19**, 1759-1762.

Jensen, E. J., and O. B. Toon, 1994: Ice nucleation in the upper troposphere: Sensitivity to aerosol number density, temperature, and cooling rate, *Geophys. Res. Lett.*, **21**, 2019-2022.

Jensen, E. J., O. B. Toon, D. L. Westphal, S. Kinne, and A. J. Heymsfield, 1994a: Microphysical modeling of cirrus 1. Comparison with 1986 FIRE IFO measurements, *J. Geophys. Res.*, **99**, 10,421-10,442.

Jensen, E. J., O. B. Toon, D. L. Westphal, S. Kinne, and A. J. Heymsfield, 1994b: Microphysical modeling of cirrus 2. Sensitivity studies, *J. Geophys. Res.*, **99**, 10,443-10,454.

Jensen, E. J., and Coauthors, 1998: Ice nucleation processes in upper tropospheric wave-clouds observed during SUCCESS, *Geophys. Res. Lett.*, **25**, 1363-1366.

Khvorostyanov, V., and K. Sassen, 1998a: Cirrus cloud simulation using explicit microphysics and radiation. Part I: Model description, *J. Atmos. Sci.*, **55**, 1808-1821.

Khvorostyanov, V., and K. Sassen, 1998b: Toward the theory of homogeneous nucleation and its parameterization for cloud models, *Geophys. Res. Lett.*, **25**, 3155-3158.

Khvorostyanov, V., and K. Sassen, 1998c: Cloud model simulation of a contrail case study: Surface cooling against upper tropospheric warming, *Geophys. Res. Lett.*, **25**, 2145-2148.

Koop, T., H. P. Ng, L. T. Molina and M. J. Molina, 1998: A new optical technique to study

aerosol phase transitions: The nucleation of ice from H_2SO_4 aerosols, *J. Phys. Chem.*A, **102**, 8924-8931.

Krueger, S. K., Q. Fu, K. N. Liou and H.-N. S. Chin, 1995: Improvements of an ice-phase microphysics parameterization for use in numerical simulations of tropical convection, *J. Appl. Meteor.*, **34**, 281-287.

Lide, D. R. (Ed.), 1998: *CRC Handbook of Chemistry and Physics*, 79th ed.,CRC Press, Boca Raton, Fla..

Lin, R.-F., 1997: A numerical study of the evolution of nocturnal cirrus by a two-dimensional model with explicit microphysics, Ph.D. thesis, 199 pp., Pennsylvania State University, University Park.

Lin, H., K. J. Noone, J. Ström, and A. J. Heymsfield, 1998: Small ice crystals in cirrus clouds: A model study and comparison with in situ observations, *J. Atmos. Sci.*, **55**, 1928-1939.

Liou, K.-N., 1986: Influence of cirrus clouds on weather and climate processes- A global perspective, *Mon. Weather Rev.*, , **114**, 1167-1199.

McFarquhar, G. M., and A. J. Heymsfield, 1998: The definition and significance of an effective radius for ice clouds, *J. Atmos. Sci.*, **55**, 2039-2052.

Meyers, P. J., P. J. DeMott, and W. R. Cotton, 1992: New primary ice-nucleation parameterizations in an explicit cloud model, *J. Appl. Meteor.*, **31**, 708-721.

Mordy, W., 1958: Computations of the growth by condensation of a population of cloud droplets, *Tellus*, **11**, 16-44.

Myhre, C. E. L., C. J. Nielsen, and O. W. Saastad, 1998: Density and surface tension of aqueous H_2SO_4 at low temperature, *J. Chem. Eng. Data*, **43**, 617-622.

Pruppacher, H. R., and J. D. Klett, 1997: *Microphysics of Clouds and Precipitation, 2nd Ed.* 954 pp., Kluwer Academic Publishers, Dordrecht.

Pruppacher, H. R., 1995: A new look at homogeneous ice nucleation in supercooled water drops, *J. Atmos. Sci.*, **52**, 1924-1933.

Ramanathan, V., R. D. Cess, E. F. Harrison, P. Minnis, B. R. Barkstrom, E. Ahmad and D. Hartmann, 1989: Cloud-radiative forcing and climate- results from the Earth Radiation Budget Experiment, *Science*, **243**, 57-63.

Rogers, D. C., P. J. DeMott, S. M. Kreidenweis, and Y. Chen, 1998: Measurements of ice nucleating aerosols during SUCCESS, *Geophys. Res. Lett.*, **25**, 1383-1386.

Rokicki, M. L., and K. C. Young, 1978: The initiation of precipitation in updrafts, *J. Appl. Meteor.*, **17**, 745-754.

Sassen, K., and S. Benson, 2000: Ice nucleation in cirrus clouds: A model study of the homogeneous and heterogeneous modes, *Geophys. Res. Lett.*, , **27**, 521-524.

Sassen, K., and G. C. Dodd, 1988: Homogeneous nucleation rate for highly supercooled cirrus cloud droplets, *J. Atmos. Sci.*, **45**, 1357-1369.

Sassen, K., and G. C. Dodd, 1989: Haze particle nucleation simulations in cirrus clouds, and applications or numerical and lidar studies, *J. Atmos. Sci.*, **46**, 3005-3014.

Spice, A., D. W. Johnson, P. R. A. Brown, A. G. Darlison, and C. P. R. Saunders, 1999: Primary ice nucleation in orographic cirrus cloud: A numerical simulation of the microphysics, *Q. J. R. Meteorol. Soc.*, , **125**, 1637-1667.

Starr, D. O'C., and G. C. Cox, 1985: Cirrus clouds. Part I: A cirrus cloud model, *J. Atmos. Sci.*, **42**, 2663-2681.

Starr, D. O'C., and Coauthors, 2000: Comparison of cirrus cloud models: A project of the

GEWEX cloud system study (GCSS) working group on cirrus cloud systems, *13th International Conf. on Clouds and Precipitation*, Aug 14-18, Reno, Nevada.

Tabazadeh, A., S. T. Martin, and J. S. Lin, 2000: The effect of particle size and nitric acid uptake on the homogeneous freezing of aqueous sulfuric acid particles, *Geophys. Res. Lett.*, **27**, 1111-1114.

Young, K. C., 1993: *Microphysical Processes in Clouds.* 427 pp., Oxford University Press, Inc., New York, New York.

R.-F. Lin, UMBC/GEST Center, NASA/Goddard Space Flight Center, Code 912, Greenbelt, MD 20771

D. O'C. Starr, Laboratory of Atmosphere, NASA/Goddard Space Flight Center, Code 912, Greenbelt, MD 20771

P. J. DeMott, Department of Atmospheric Sciences, Colorado State University, Fort-Collins, CO 80523-1371

R. Cotton, Meteorological Research Flight, DERA Farnborough, Hants, GU14 6TD, UK

K. Sassen, Department of Meteorology, University of Utah, Salt Lake City, UT 84112

E. Jensen, NASA/Ames Research Center, Moffett Field, CA 94035

Received _____

Figure 1. The flowchart of a typical cirrus parcel model.

Figure 2. Homogeneous nucleation rate times equilibrium-sized haze volume $J_{haze}V$ versus temperature is shown for sulfuric acid haze particles with solute mass 10^{-13}g when the solute wt% are 5, 15, and 25%. Homogeneous nucleation takes place between -43.2 to -44.2°C and -63.2 to -64.2°C in simulations Wh020L and Ch020L, respectively (illustrated by brackets). Model C (dashed lines), S (dashed-dotted lines), and models D and L (dotted lines) compute J_w using fitted or theoretical equations from (Jeffery and Austin 1997), (Khvorostyanov and Sassen 1998b), and (Heymsfield and Miloshevich 1993), respectively. Model J (solid lines) adopts the modified classical approach.

Figure 3. Melting point depression (ΔT_m) of H_2SO_4 solution as a function of solute wt% from the tabular data of *CRC Handbook of Chemistry and Physics*, Ed. 79. The solid and unfilled diamond markers denote tabular data points from pp. 8-81 and pp. 15-22, respectively. Also plotted are curves of $\lambda\Delta T_m$ for λ=1, 1.5, 1.7, 2.0. The solid and unfilled right triangle markers indicate inferred $\lambda\Delta T_m$ from model J at T = -65 and -45°C, respectively.

Figure 4. H_2SO_4 solution density as a function of solute wt%. Also shown in the figure is H_2SO_4 solution density at -45°C fitted by Myhre et al. (1998). The tabular data of *CRC Handbook of Chemistry and Physics* for H_2SO_4 solution density at 20°C matches well with the curve of model D.

Figure 5. Solute wt% of haze particles in equilibrium with the environment as a function of water relative humidity RH_w for solute mass 10^{-12}, 10^{-13}, 10^{-14}, 10^{-15}g. The solid and the dotted lines indicate results from models C and L, respectively. Also shown are the solute wt% and RH_w of particles that satisfy the critical freezing condition at temperatures -65 and -45°C by the five participant models. The values of λ used are listed in Table 2. The four markers sizes from the biggest to the smallest indicate solute mass 10^{-12}, 10^{-13}, 10^{-14}, 10^{-15}g, accordingly. Homogeneous nucleation takes place between 95.5 and 98% and 85.5 and 91% in simulations Wh020L and Ch020L, respectively. These two moisture ranges are also bracketed in this plot.

Figure 6. Haze particle solute wt% versus solute mass by model C just before homogeneous nucleation is triggered.

Figure 7. The evolution of IWC, ice number concentration, relative humidity wrt. ice, and temperature of the parcel in case Ch020. Note that z_{ini} is the initial height of the parcel.

Figure 8. Ice number concentration predicted versus imposed updraft speed. The predicted N_i of the HN-ONLY runs is denoted by unfilled bars, while that of the ALL-MODE simulations is indicated by color-filled bars. The marker "X" indicate that homogeneous nucleation is not triggered in the ALL-MODE run. Note that model J did not submit the ALL-MODE results.

Figure 9. The RH_i at cloud base z_b and the corresponding Δ RH_i, defined as the difference between peak RH_i and RH_i at cloud base z_b.

Figure 10. The same as Fig. 7 except for case Ca020.

Figure 11. Ice water content, ice number concentration, ice particle formation rate $\frac{dN_i}{dt}$, and RH_w as functions of $z - z_b$, where z_b is the altitude where nucleation starts ($N_i = 10^{-3}$ cc^{-1}). The line and marker conventions are the same as those in Fig. 7.

Figure 12. The number distribution of the haze particles frozen in the lifting process. The initial haze number distribution is denoted by the thin solid curves.

Figure 13. The same as Fig. 11 except this is a sensitivity test on β_i performed by model L.

Figure 14. Ice water content versus N_i. Note that the parcel height increment between two consecutive markers is 5 m.

Figure 15. Volume absorption coefficient at wavelength 10.75 μm (panels [a] and [e]), effective radius (panels [b] and [f]), mass weighted ice terminal velocity (panels [c] and [g]) at 800 m above the starting point of the simulations, and the time interval between peak RH_i achieved by the parcel and the equilibrium RH_i (panels [d] and [h]). The filled bars indicate ALL-MODE simulations while the unfilled bars denote HN-ONLY simulations.

Figure 16. The predicted ice number concentration versus the equilibrium RH_i.

Table 1. Simulation identifiers and initial conditions. $RH_{i,ini} = 100\%$ in every simulation.

	simulation identifiers		height z_{ini} (km)	pressure P_{ini} (mb)	temperature T_{ini} (°C)	updraft W (m s^{-1})	Lapse rate Γ (°C m^{-1})
	All-MODE	HN-ONLY					
warm	Wa004	Wh004	8.3	340	-40	0.04	0.093
cases[a]	Wa020	Wh020	8.3	340	-40	0.20	0.093
	Wa100	Wh100	8.3	340	-40	1.00	0.093
cold	Ca004	Ch004	13.4	170	-60	0.04	0.097
cases[a]	Ca020	Ch020	13.4	170	-60	0.20	0.097
	Ca100	Ch100	13.4	170	-60	1.00	0.097
λ-fixed[b]		Wh020L	8.3	340	-40	0.20	0.093
		Ch020L	13.4	170	-60	0.20	0.097

[a] λ, if any, is determined by the participants.

[b] $\lambda = 2$. Note that model J incorporates parameters adjusted to the laboratory data of Koop et al. (1998) in all λ-fixed and HN-ONLY cases.

Table 2. Participant cirrus parcel models.

Organization	UKMO	CSU	ARC	GSFC	U. Utah
Investigator	Cotton (C)	DeMott (D)	Jensen (J)	Lin (L)	Sassen (S)
Time step (s)	0.01	10/W (W in cm/s)	adjusting 10^{-5} to 0.02	0.02	0.01
Ice number distribution					
Bin number	30	32	60	25	no binning,
Bin characteristic[a]	discrete	continuous	continuous	continuous	particle tracing
Bin advection	Lagrangian Darlison (1988)	Lagrangian Rokicki and Young (1978)	Eulerian Colella and Woodward (1984)	Lagrangian Chen and Lamb (1994)	Lagrangian
Haze number distribution					
Bin number	20	100	60	20	20
Haze size[b]	r_{eq} or $\frac{dr}{dt}$	r_{eq}	r_{eq}	r_{eq} or $\frac{dr}{dt}$	r_{eq} or $\frac{dr}{dt}$
Homogeneous nucleation					

Table 2. (continued)

Organization	UKMO	CSU	ARC	GSFC	U. Utah
Investigator	Cotton (C)	DeMott (D)	Jensen (J)	Lin (L)	Sassen (S)
T_{eff}	yes	yes	no	yes	yes
λ^{c}	1.5	1.5		1.0	1.7
β_i^{d}	0.24	0.04	1	0.1	0.36
Heterogeneous nucleation	S_i dependent deposition nucleation	immersion freezing nucleation	not submitted	S_i dependent deposition nucleation	T_{eff} dependent modified Fletcher eq.
References	Spice et al. (1999)	DeMott et al. (1994a) DeMott et al. (1998)	Jensen et al. (1994) Tabazadeh et al. (2000)	Lin (1997)	Sassen and Dodd (1988) Khvorostyanov and Sassen (1998b)

[a]Discrete versus continuous binning indicates if assuming that particles have exactly the same size in a bin or it allows a certain size distribution of particles in a bin.

[b]Note that r_{eq} versus $\frac{dr}{dt}$ denotes either using the equilibrium-sized haze approximation or computing the diffusional growth of haze particles explicitly.

[c]Native value of λ assumed in model.

[d]β_i is the deposition coefficient.

Table 3. N_i reduction ratio, which is defined as N_i of the ALL-MODE divided by N_i of the HN-ONLY simulation, $N_{i,ALL-MODE}/N_{i,HN-ONLY}$.

Model	C	D	L	S
Simulation	N_i reduction ratio.			
Ca004	0.039	0.849	0.091	6.500
Ca020	0.114	0.958	0.073	0.137
Ca100	0.791	0.979	0.901	0.177
Wa004	0.083	0.079	0.190	0.667
Wa020	0.036	0.825	0.108	0.283
Wa100	0.524	0.931	0.559	0.287

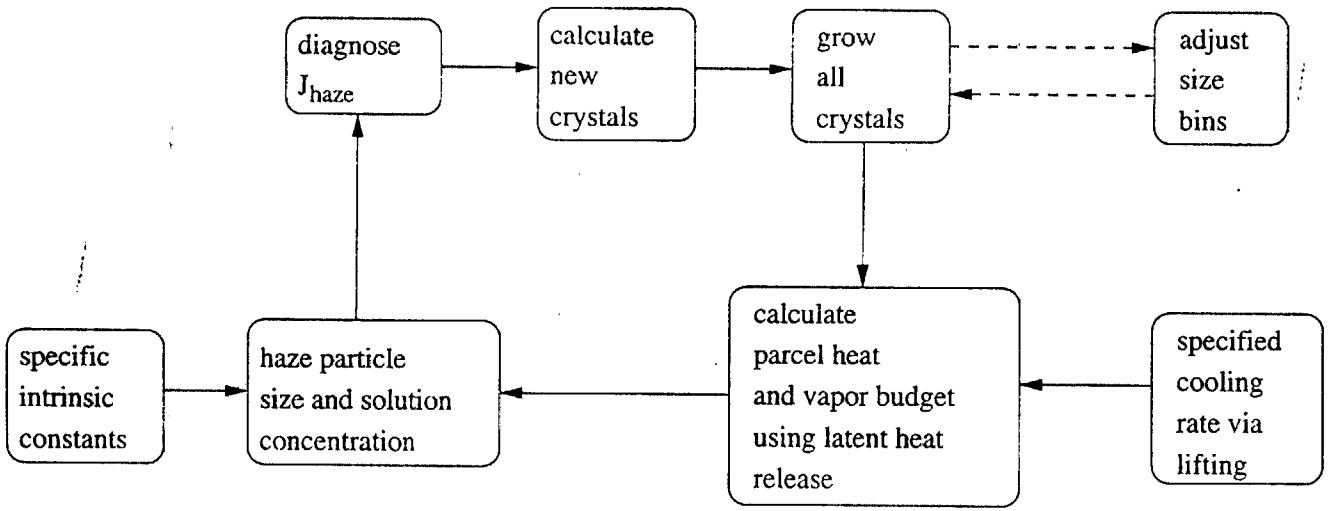

Figure 1. The flowchart of a typical cirrus parcel model.

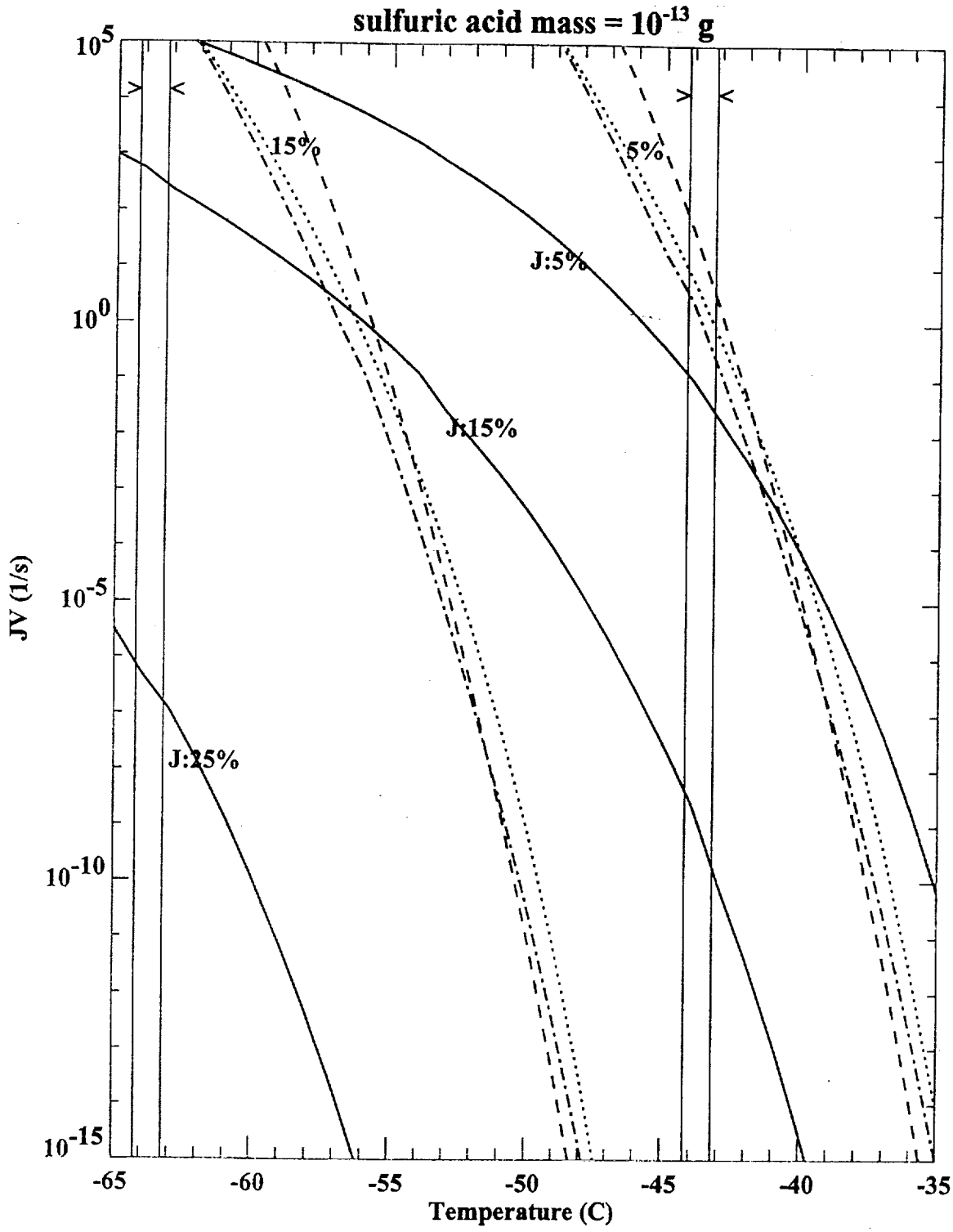

Figure 2. Homogeneous nucleation rate times equilibrium-sized haze volume $J_{haze}V$ versus temperature is shown for sulfuric acid haze particles with solute mass 10^{-13}g when the solute wt% are 5, 15, and 25%. Homogeneous nucleation takes place between -43.2 to -44.2°C and -63.2 to -64.2°C in simulations Wh020L and Ch020L, respectively (illustrated by brackets). Model C (dashed lines), S (dashed-dotted lines), and models D and L (dotted lines) compute J_w using fitted or theoretical equations from (Jeffery and Austin 1997), (Khvorostyanov and Sassen 1998b), and (Heymsfield and Miloshevich 1993), respectively. Model J (solid lines) adopts the modified classical approach.

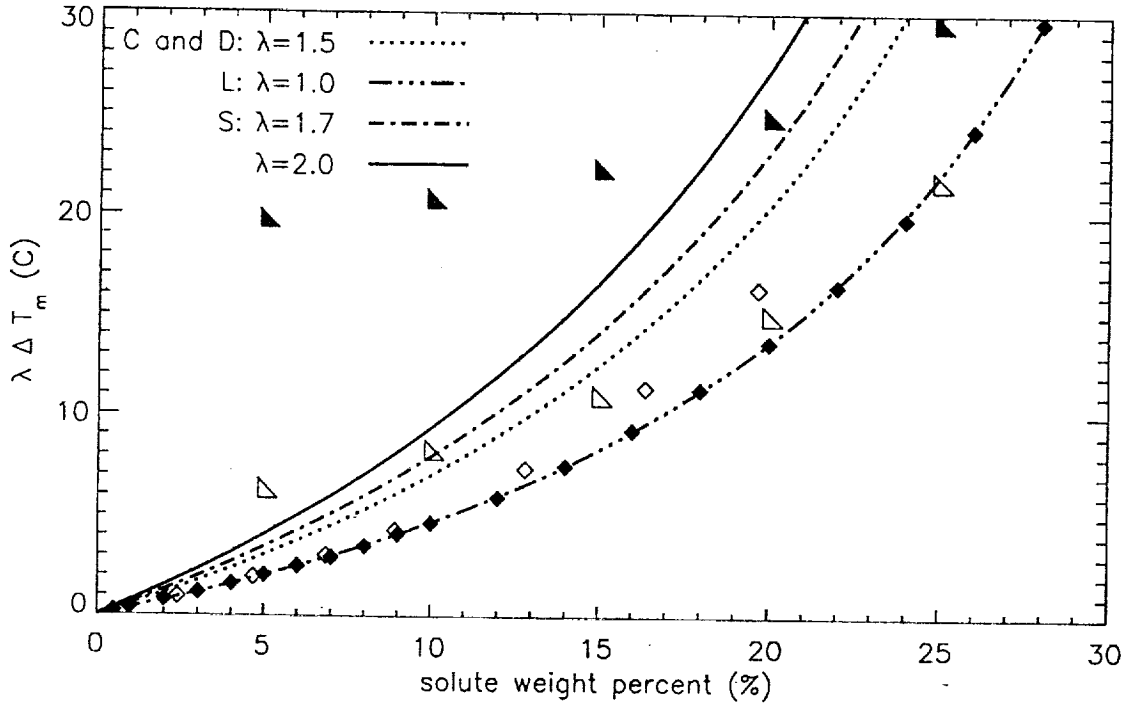

Figure 3. Melting point depression (ΔT_m) of H_2SO_4 solution as a function of solute wt% from the tabular data of *CRC Handbook of Chemistry and Physics*, Ed. 79. The solid and unfilled diamond markers denote tabular data points from pp. 8-81 and pp. 15-22, respectively. Also plotted are curves of $\lambda\Delta T_m$ for λ=1, 1.5, 1.7, 2.0. The solid and unfilled right triangle markers indicate inferred $\lambda\Delta T_m$ from model J at T = -65 and -45°C, respectively.

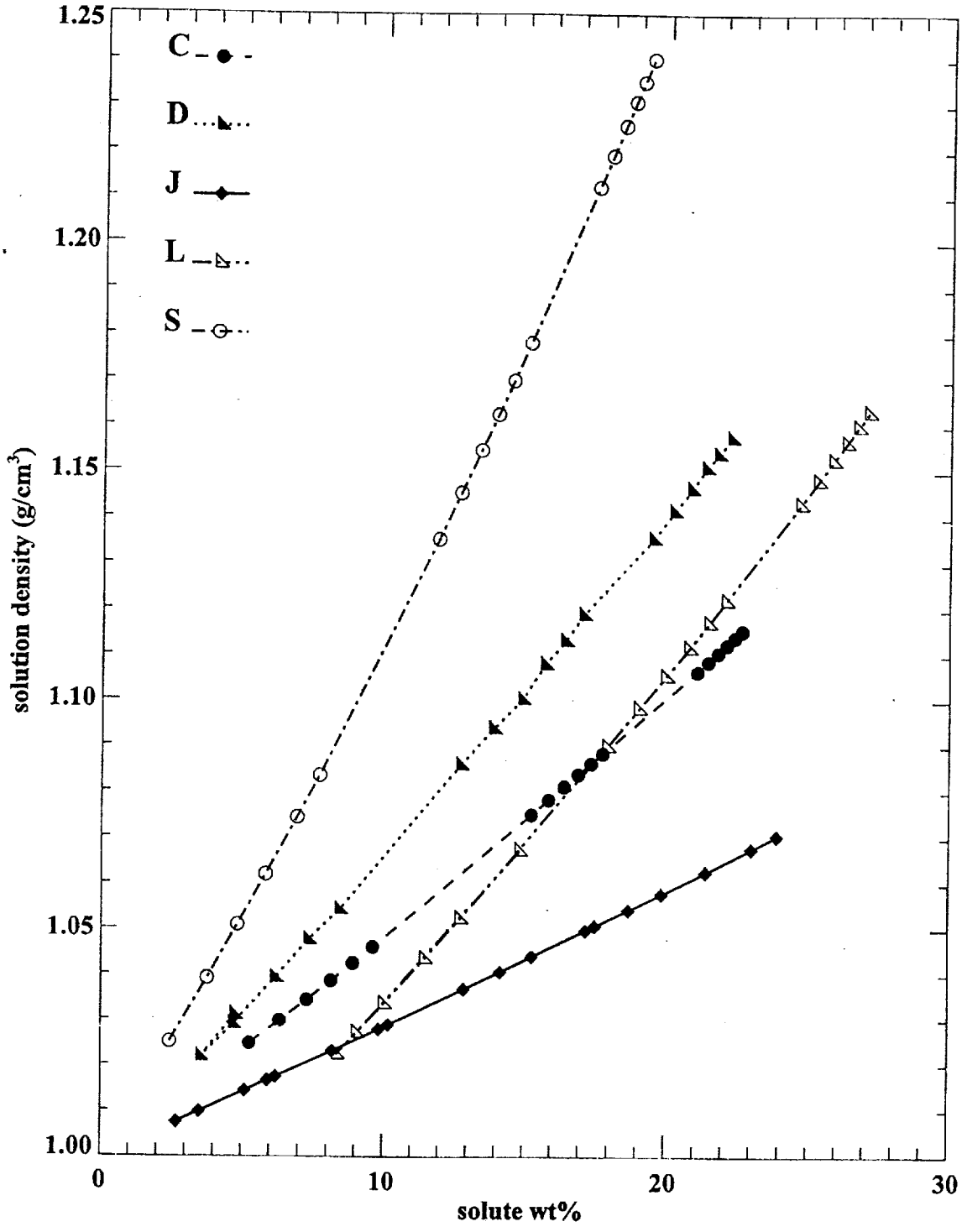

Figure 4. H_2SO_4 solution density as a function of solute wt%. Also shown in the figure is H_2SO_4 solution density at -45°C fitted by Myhre et al. (1998). The tabular data of *CRC Handbook of Chemistry and Physics* for H_2SO_4 solution density at 20°C matches well with the curve of model D.

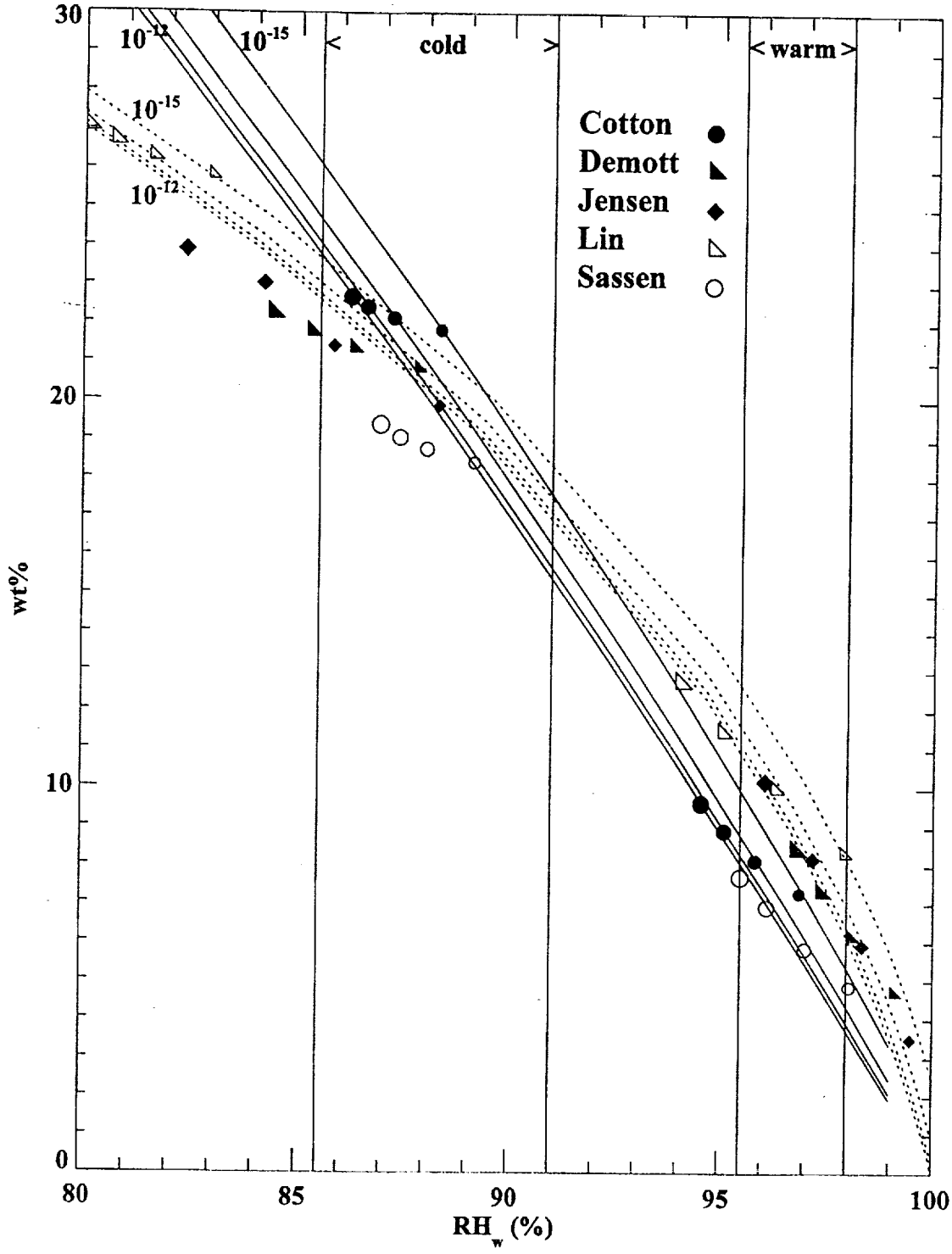

Figure 5. Solute wt% of haze particles in equilibrium with the environment as a function of water relative humidity RH_w for solute mass 10^{-12}, 10^{-13}, 10^{-14}, 10^{-15}g. The solid and the dotted lines indicate results from models C and L, respectively. Also shown are the solute wt% and RH_w of particles that satisfy the critical freezing condition at temperatures -65 and -45°C by the five participant models. The values of λ used are listed in Table 2. The four markers sizes from the biggest to the smallest indicate solute mass 10^{-12}, 10^{-13}, 10^{-14}, 10^{-15}g, accordingly. Homogeneous nucleation takes place between 95.5 and 98% and 85.5 and 91% in simulations Wh020L and Ch020L, respectively. These two moisture ranges are also bracketed in this plot.

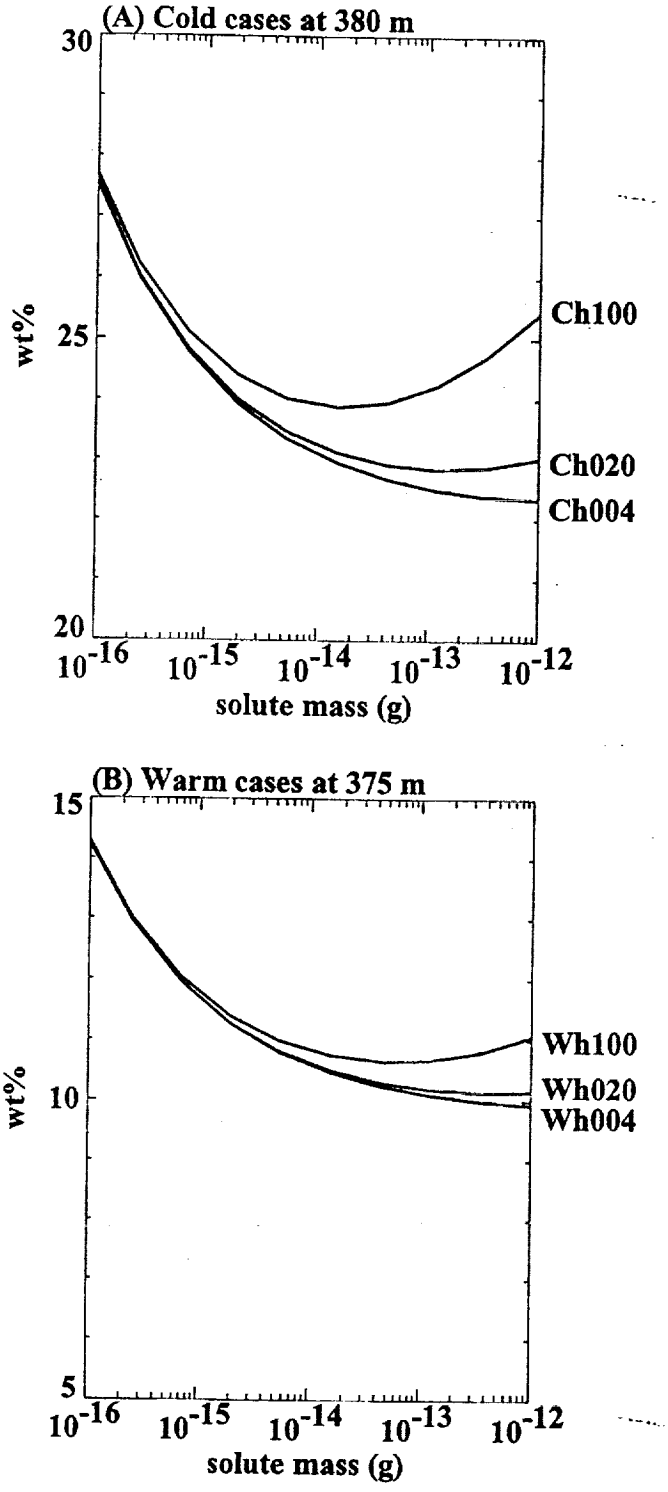

Figure 6. Haze particle solute wt% versus solute mass by model C just before homogeneous nucleation is triggered.

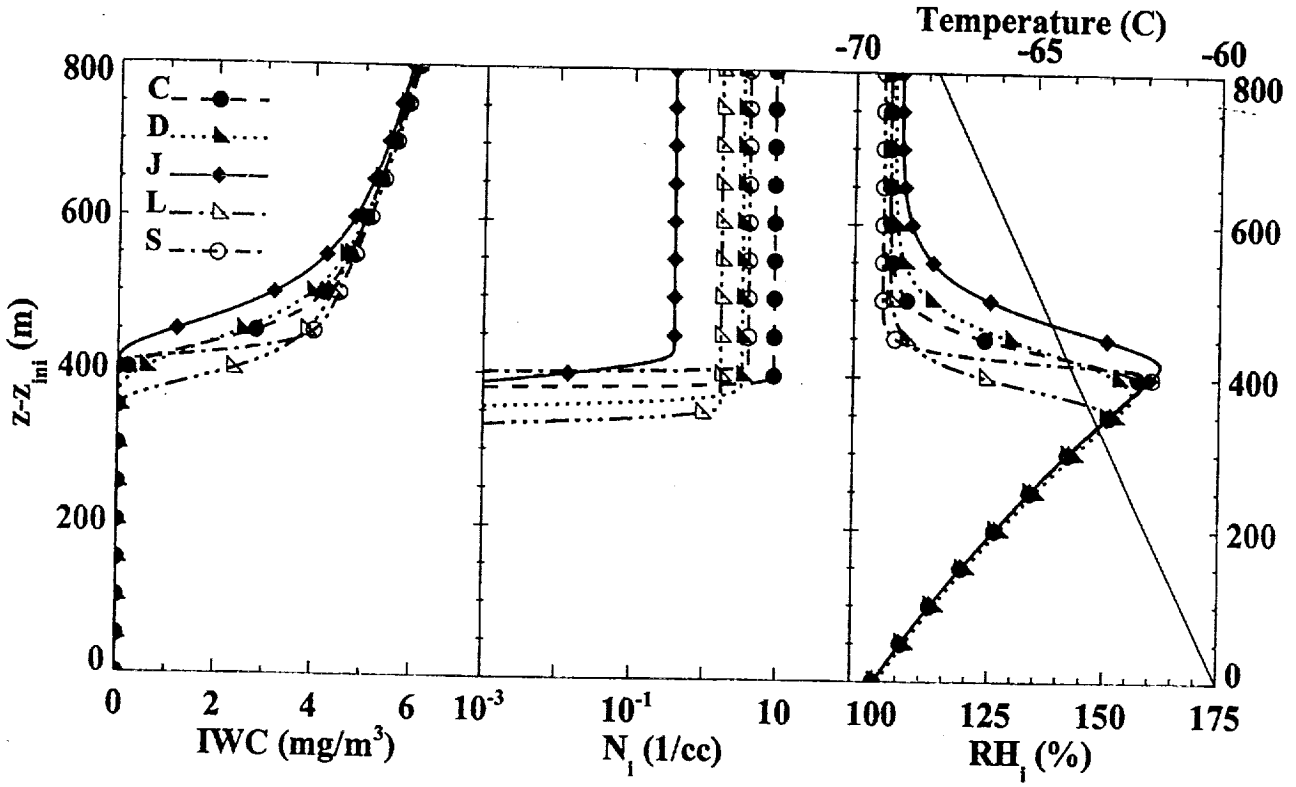

Figure 7. The evolution of IWC, ice number concentration, relative humidity wrt. ice, and temperature of the parcel in case Ch020. Note that z_{ini} is the initial height of the parcel.

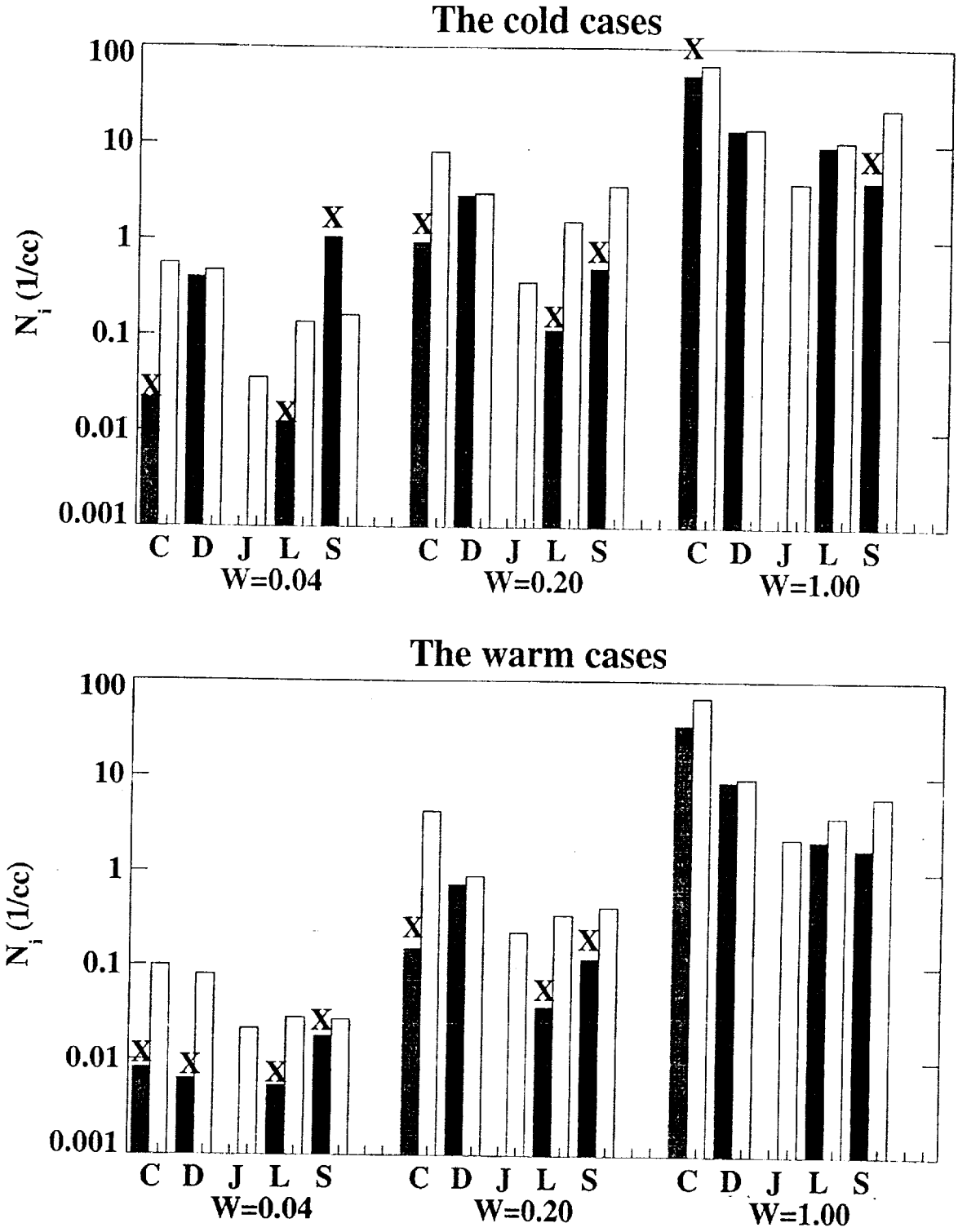

Figure 8. Ice number concentration predicted versus imposed updraft speed. The predicted N_i of the HN-ONLY runs is denoted by unfilled bars, while that of the ALL-MODE simulations is indicated by color-filled bars. The marker "X" indicate that homogeneous nucleation is not triggered in the ALL-MODE run. Note that model J did not submit the ALL-MODE results.

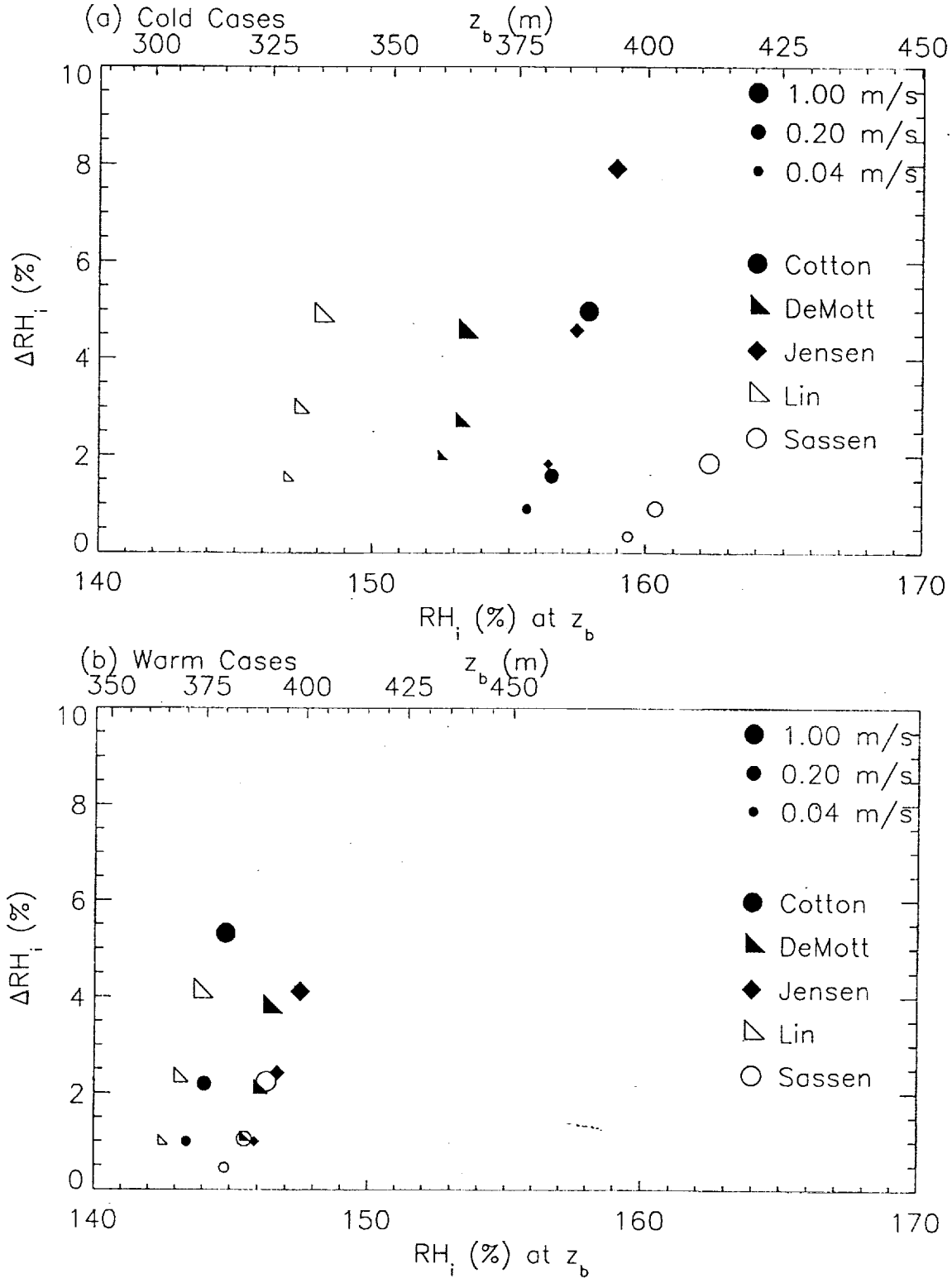

Figure 9. The RH_i at cloud base z_b and the corresponding Δ RH_i, defined as the difference between peak RH_i and RH_i at cloud base z_b.

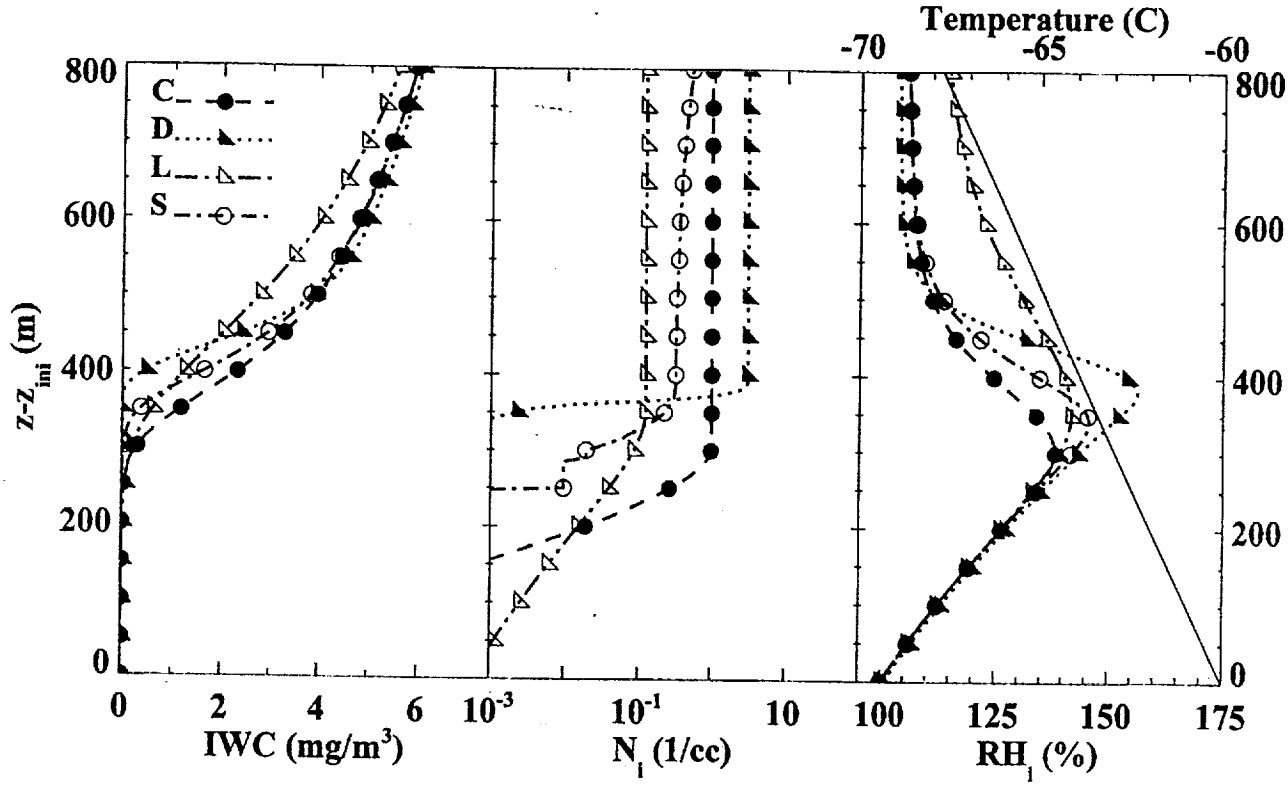

Figure 10. The same as Fig. 7 except for case Ca020.

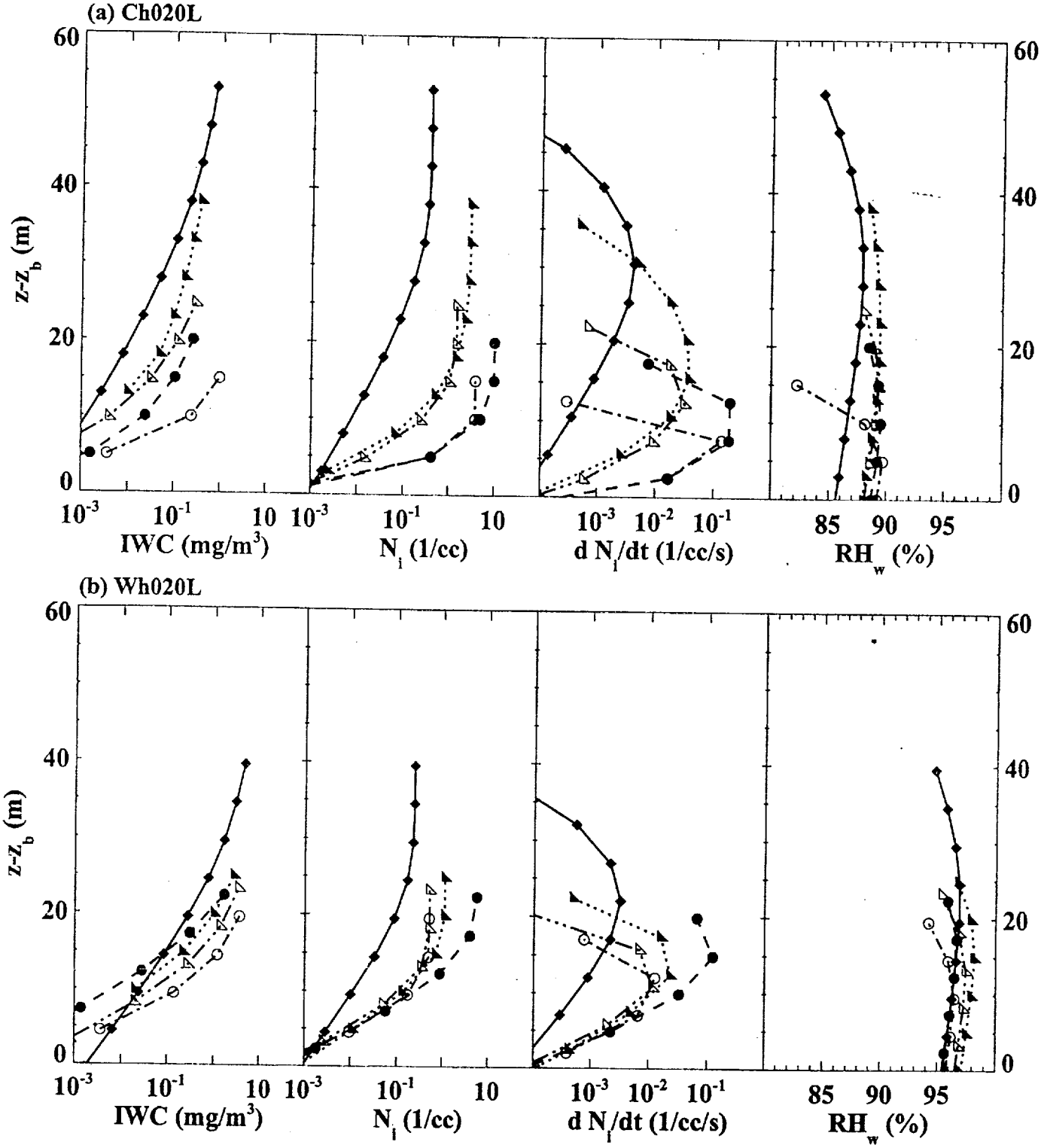

Figure 11. Ice water content, ice number concentration, ice particle formation rate $\frac{dN_i}{dt}$, and RH_w as functions of $z - z_b$, where z_b is the altitude where nucleation starts ($N_i = 10^{-3}$ cc^{-1}). The line and marker conventions are the same as those in Fig. 7.

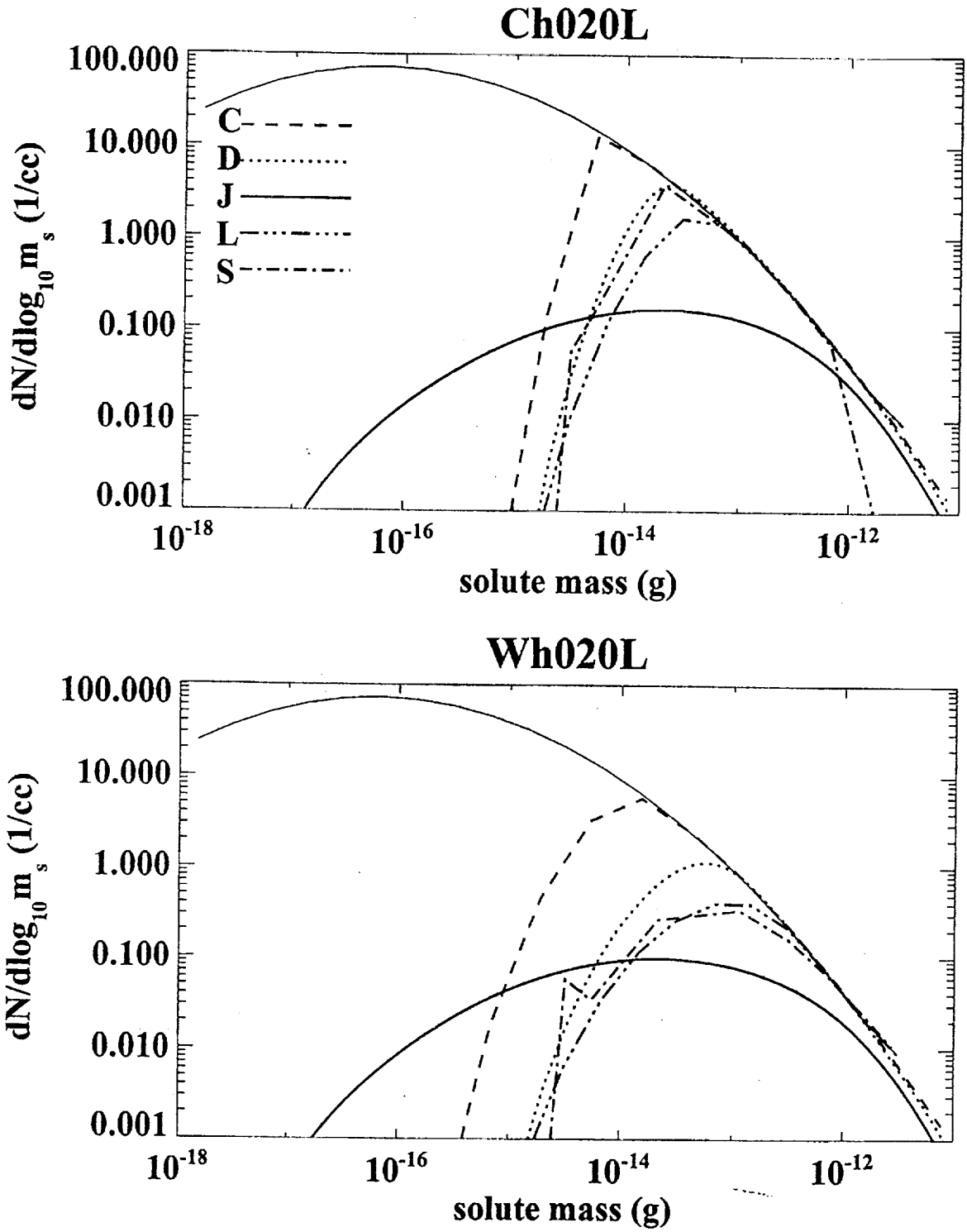

Figure 12. The number distribution of the haze particles frozen in the lifting process. The initial haze number distribution is denoted by the thin solid curves.

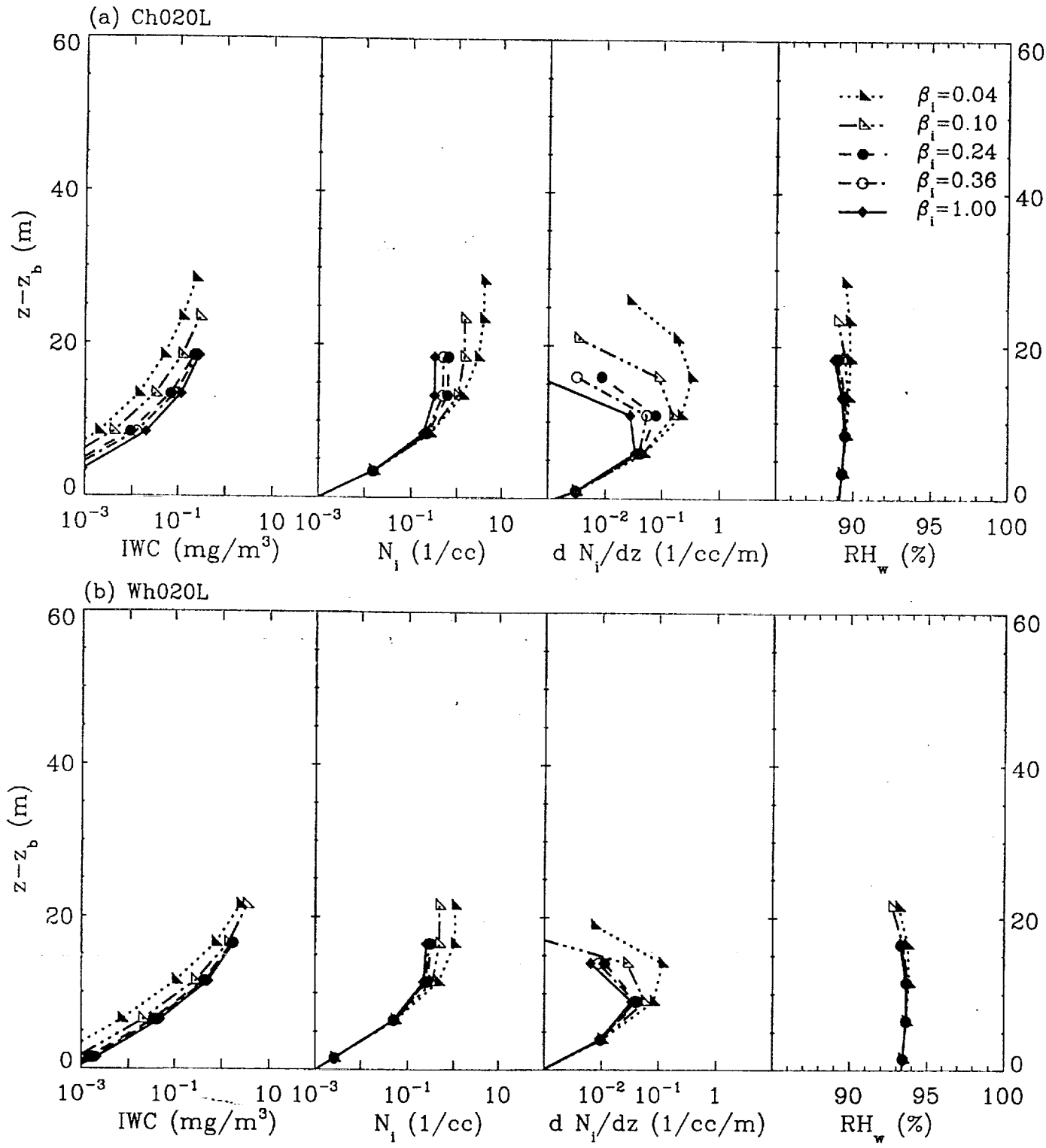

Figure 13. The same as Fig. 11 except this is a sensitivity test on β_i performed by model L.

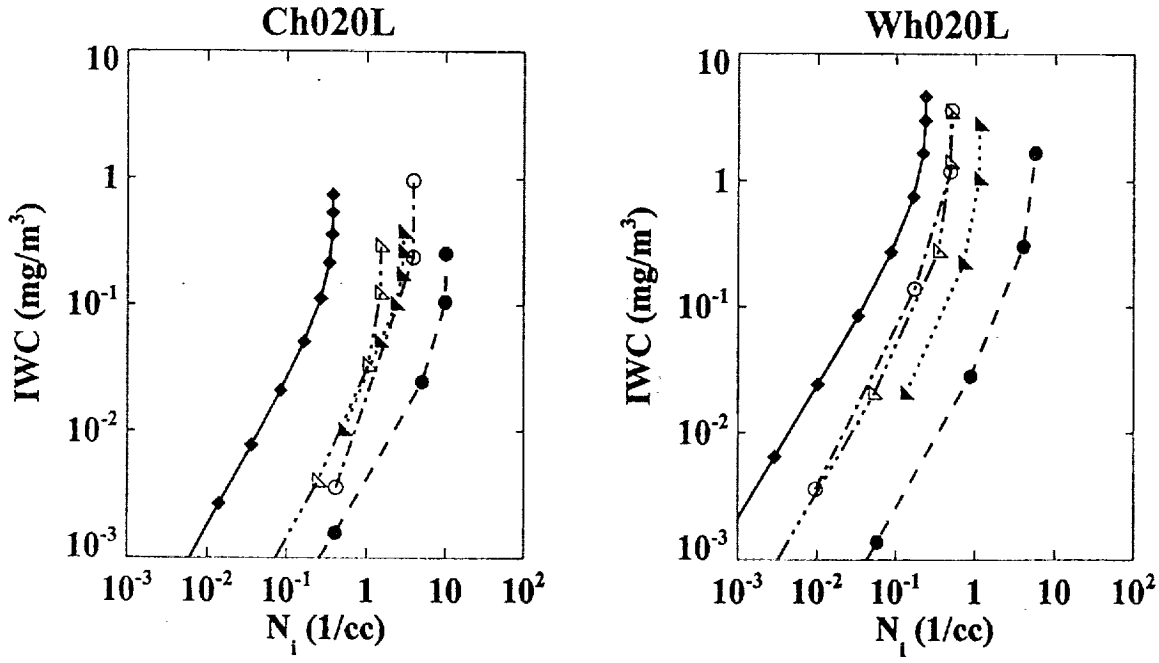

Figure 14. Ice water content versus N_i. Note that the parcel height increment between two consecutive markers is 5 m.

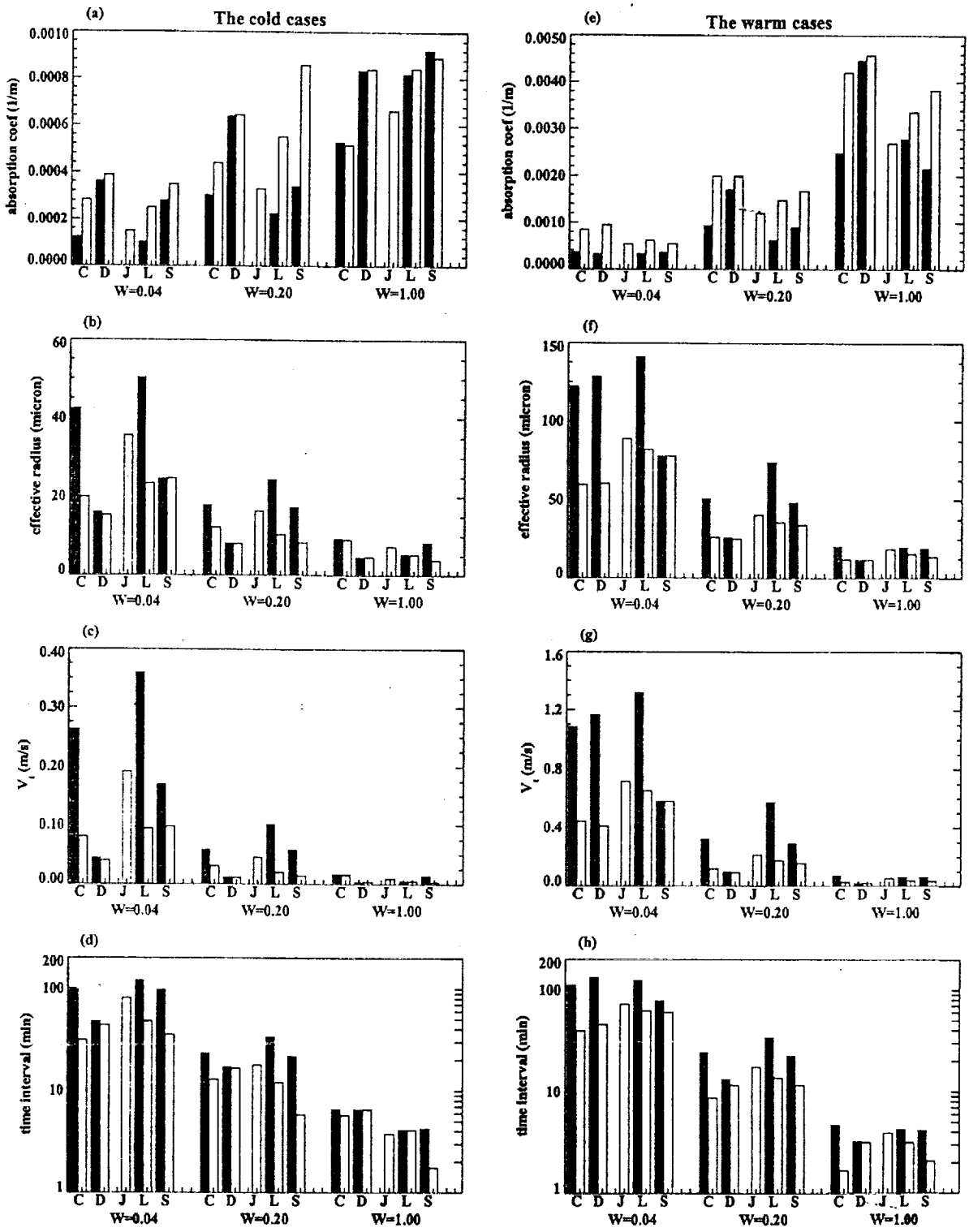

Figure 15. Volume absorption coefficient at wavelength 10.75 μm (panels [a] and [e]), effective radius (panels [b] and [f]), mass weighted ice terminal velocity (panels [c] and [g]) at 800 m above the starting point of the simulations, and the time interval between peak RH_i achieved by the parcel and the equilibrium RH_i (panels [d] and [h]). The filled bars indicate ALL-MODE simulations while the unfilled bars denote HN-ONLY simulations.

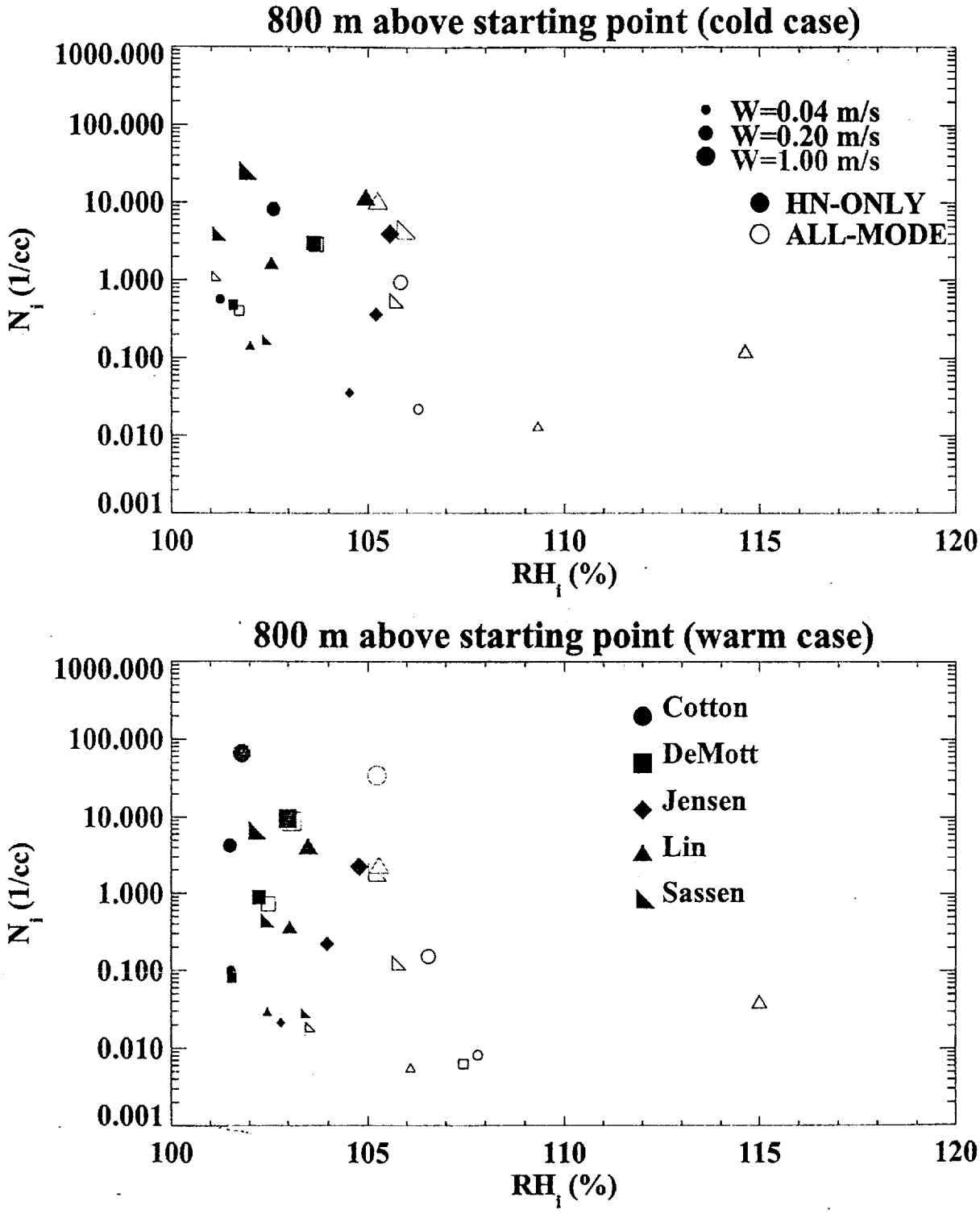

Figure 16. The predicted ice number concentration versus the equilibrium RH_i.